

## Research Paper

# Coniferaldehyde attenuates Alzheimer's pathology via activation of Nrf2 and its targets

Yaqiong Dong<sup>1</sup>, Tessandra Stewart<sup>2</sup>, Lidan Bai<sup>1</sup>, Xue Li<sup>1</sup>, Ting Xu<sup>1</sup>, Jeffrey Iliff<sup>3</sup>, Min Shi<sup>2</sup>, Danfeng Zheng<sup>4</sup>, Lan Yuan<sup>1</sup>, Taotao Wei<sup>5</sup>, Xiaoda Yang<sup>1</sup>✉, and Jing Zhang<sup>2,4</sup>✉

1. The State Key Laboratories of Natural and Biomimetic Drugs and Department of Chemical Biology, School of Pharmaceutical Sciences, Peking University Health Science Center, Beijing 100191, China
2. Department of Pathology, University of Washington School of Medicine, Seattle, WA 98104, United States
3. Department of Anesthesiology and Perioperative Medicine, Knight Cardiovascular Institute, Oregon Health & Science University, Portland, OR, United States
4. Department of Pathology, School of Basic Medical Sciences, Peking University Health Science Center, Beijing 100191, China
5. National Laboratory of Biomacromolecules, Institute of Biophysics, Chinese Academy of Sciences, Beijing 100101, China

✉ Corresponding author: Prof. Jing Zhang, Department of Pathology, University of Washington School of Medicine, Seattle, WA 98104, United States, E-mail: zhangj@uw.edu; or Prof. Xiaoda Yang, the State Key Laboratories of Natural and Biomimetic Drugs and Department of Chemical Biology, School of Pharmaceutical Sciences, Peking University Health Science Center, Beijing 100191, China, E-mail: xyang@bjmu.edu.cn

© The author(s). This is an open access article distributed under the terms of the Creative Commons Attribution License (<https://creativecommons.org/licenses/by/4.0/>). See <http://ivyspring.com/terms> for full terms and conditions.

Received: 2019.05.15; Accepted: 2019.09.02; Published: 2020.01.01

## Abstract

**Background:** Alzheimer's disease (AD) currently lacks a cure. Because substantial neuronal damage usually occurs before AD is advanced enough for diagnosis, the best hope for disease-modifying AD therapies likely relies on early intervention or even prevention, and targeting multiple pathways implicated in early AD pathogenesis rather than focusing exclusively on excessive production of  $\beta$ -amyloid ( $A\beta$ ) species.

**Methods:** Coniferaldehyde (CFA), a food flavoring and agonist of NF-E2-related factor 2 (Nrf2), was selected by multimodal *in vitro* screening, followed by investigation of several downstream effects potentially involved. Furthermore, in the APP/PS1 AD mouse model, the therapeutic effects of CFA ( $0.2 \text{ mmol kg}^{-1} \text{ d}^{-1}$ ) were tested beginning at 3 months of age. Behavioral phenotypes related to learning and memory capacity, brain pathology and biochemistry, including  $A\beta$  transport, were assessed at different time intervals.

**Results:** CFA promoted neuron viability and showed potent neuroprotective effects, especially on mitochondrial structure and functions. In addition, CFA greatly enhanced the brain clearance of  $A\beta$  in both free and extracellular vesicle (EV)-contained  $A\beta$  forms. In the APP/PS1 mouse model, CFA effectively abolished brain  $A\beta$  deposits and reduced the level of toxic soluble  $A\beta$  peptides, thus eliminating AD-like pathological changes in the hippocampus and cerebral cortex and preserving learning and memory capacity of the mice.

**Conclusion:** The experimental evidence overall indicated that Nrf2 activation may contribute to the potent anti-AD effects of CFA. With an excellent safety profile, further clinical investigation of coniferaldehyde might bring hope for AD prevention/therapy.

Key words: Alzheimer's disease;  $A\beta$  clearance; coniferaldehyde; neuroprotection; Nrf2

## Introduction

The escalating prevalence of Alzheimer's disease (AD) presents an enormous world-wide challenge to patients, as well as a significant social and economic burden [1]. However, to date, a variety of efforts for

disease-modifying therapy have failed [2, 3]. Most therapies are based on the  $A\beta$ -Tau cascade hypothesis, the leading theory to explain AD pathophysiology [4, 5]. However,  $A\beta$  accumulation

occurs over a long period, beginning as much as 10-20 years before the appearance of clinical symptoms [6]. Thus, treatment at symptomatic stages might be too late because irreversible damage to neurons has already occurred [7, 8]. Hence, treating AD at early stages and targeting processes upstream of AD pathogenesis, such as amyloid  $\beta$  ( $A\beta$ ) deposition to prevent the onset of AD pathology in the brain, might be a more desirable strategy [8-12].

Because AD pathogenesis is likely dependent on simultaneous dysfunction of multiple pathways [13, 14], identification of therapeutic agents capable of multi-modal targeting of disparate processes in parallel, especially at early stages, might be more efficient in preventing neuronal death and preserving cognitive function. Potential targets include removal of  $A\beta$  species, especially the toxic soluble  $A\beta$  oligomers [4, 15, 16], from the CNS, a process that is dramatically reduced in AD [17]; mitochondrial dynamics and metabolism, which have been suggested as among the earliest manifestations of AD [18, 19]; and neurotrophic or similar functions, which when promoted by some compounds can reverse cognitive impairment in AD animals even without reducing the senile plaques [20]. Therefore, we sought novel, disease-modifying agents for treatment of AD by simultaneous targeting of multiple pathways, i.e. improvement of neural cell viability and neuroprotection, particularly against mitochondrial dysfunction, from compounds with known safety profiles and promotion of brain  $A\beta$  clearance. To achieve this goal, we considered activators of NF-E2-related factor 2 (Nrf2), a master regulator of major cellular defense systems responsible for promoting expression of enzymes that protect against oxidative stress and efflux transporters [21-24]. Importantly, inactivation of Nrf2 has been shown to be tightly linked to AD [25, 26]. Therefore, we proposed that an effective AD disease-modifying agent may be found by screening Nrf2 agonists.

Based on the activity of cinnamaldehyde, which enhances mitochondrial function while reducing  $A\beta$  oligomerization and Tau aggregation [27, 28], we conducted a screening of a variety of cinnamaldehyde analogs, which have the  $\alpha,\beta$ -unsaturated carbonyl group that serves as a potent activator of Nrf2, and identified coniferaldehyde (CFA) (Fig. 1A), a food flavoring [29, 30], that met all of these criteria. CFA effectively promoted neuronal cell viability and provided strong neuroprotective effects to neuronal cells under stress due to elevated levels of  $A\beta$  or exposure to mitochondrial toxins, improved mitochondrial function, and significantly enhanced brain excretion of both free and extracellular vesicle (EV)-bound forms of  $A\beta$ . Further, CFA gave

reassuring results in preservation of learning and memory function in AD model animals and substantial reduction of brain  $A\beta$  pathology. Overall, our results suggest CFA is a promising putative preventive/therapeutic agent for AD.

## Materials and Methods

### Materials

Coniferaldehyde (CFA) (98%) and Tretinoin (ATRA) were from Sigma Aldrich Tech Co. (USA). 3-(4,5-dimethylthiazol-2-yl)-5-(3-carboxymethoxyphenyl)-2-(4-sulfophenyl)-2H-tetrazolium (MTS) was from Promega (USA). Arabinoside Cytosine (AraC) and Poly-D-lysine were from Sigma Aldrich Tech Co. (USA). Neurobasal-A medium and Glutamine were from Invitrogen (USA). Minimum Essential Medium Non-Essential Amino Acids (MEM, NEAA) Solution, B-27 and fetal bovine serum (FBS) were from Gibco (USA). Dulbecco's modified Eagle's medium (DMEM) and phosphate buffer saline (PBS) were from Hyclone (USA). Penicillin/streptomycin, MitoTracker Red CMXRos was from Invitrogen (USA). XF Cell Mito Stress Test Kit and XF Glycolysis Stress Test Kit were from Seahorse Bioscience (USA). Reactive Oxygen (ROS) Species Assay Kit and Bicinchoninic Acid (BCA) Protein Quantitation Kit were from Beyotime (China). Mitochondrial Membrane Potential Assay Kit with JC-1 was from Bridgen (China). ATP Bioluminescence Assay Kit was from Beyotime (China). Nrf2 siRNA was from Santa Cruz (USA). Lipofectamine™ 3000 Transfection Reagent was from Thermo Fisher (USA). Primary antibodies:  $A\beta_{1-16}$  (6E10) from Biogen (USA), MAP2, GFAP, Nrf2, HO-1, Drp1, PKM2, p-Tau (ser 262, ser 422), p-GSK-3 $\beta$  (ser 9), p-AKT (ser 473) from Abcam (USA). Goat anti-Rabbit IgG (H+L) Highly Cross-Adsorbed Secondary Antibody (Alexa Fluor 488) was from Abcam (USA). GAPDH and HRP-conjugated anti-mouse and anti-rabbit secondary antibodies were from Easybio (China). Dimethylsulfoxide (DMSO) was from Sigma Aldrich Tech Co. (USA). Other reagents were of analytical grade.

### Cell culture and treatment

Three human neuroblastoma SH-SY5Y cell lines (neo, APPwt, and APPswe) were obtained from Institute of Biophysics, Chinese Academy of Sciences; the SH-SY5Y APPwt cells express wild type  $A\beta$  precursor protein (APP); SH-SY5Y APPswe cells express APP with the Swedish mutation; SH-SY5Yneo are the blank cells transfected with an empty vector. SH-SY5Yneo cells produce marginal levels of  $A\beta$  peptides while the SH-SY5Y APPswe cells generate high concentrations of  $A\beta$  up to 1000 pg/ml [31]. The cells were cultured in DMEM supplemented with 10%

FBS, 1% MEM NEAA, 1% penicillin/streptomycin, 5% CO<sub>2</sub> atmosphere at 37 °C. These cells were kept selected by G418 resistance.

To observe the effect of CFA on mitochondrial intoxication, SH-SY5Y cells were pretreated with 300 μM MPP<sup>+</sup> or 1 μM Rotenone for 24 h. The cells were cultured in DMEM/F12 supplemented with 10% FBS, 1% penicillin/streptomycin, 5% CO<sub>2</sub> atmosphere at 37 °C.

CFA stock solutions were prepared in DMSO, and freshly diluted with culture medium to the working concentrations. After pre-incubation of cells at 37 °C for 24 h, desired concentrations of CFA were added and incubated for 36 h at 37 °C before conducting assays.

### Cell viability

Cell viability was evaluated by MTS assay [32]. Briefly, cells (5×10<sup>3</sup> cells/well) were seeded into 96-well plates and incubated for 24 h. Then various concentrations (0.1~200 μM) of CFA were added to wells. After treatment for 36 h, MTS solution diluted with DMEM at a final concentration of 0.2 mg/mL was added and incubated for another 2 h. Finally, the absorbance at 490 nm of each condition was determined on a microplate reader (Thermo Lab systems, Finland).

### Immunofluorescent observation of Nrf2 translocation into the nucleus

The SH-SY5Y cells were grown on 35-mm<sup>2</sup> confocal dishes (Axygen, USA). After treatment with 100 μM CFA for 36 h at 37 °C, the cells were in turn washed three times with PBS, fixed in 4% formaldehyde for 10-15 min, and made permeable with 1% Triton X-100. Then the cells were blocked in 1% BSA for 30 min. After blocking, the cells were incubated with primary Nrf2 antibody (1:500 dilution in blocking solution) for 3 h at room temperature. After wash, the cells were incubated with fluorescein isothiocyanate (FITC)-labeled (green) secondary antibodies (1:50) for 2 h at room temperature. The dishes were then counter stained with 40, 6-diamidino-2-phenylindole (DAPI) for 10 min and covered with 90% glycerol. The fluorescent images were observed on a confocal laser-scanning microscope (Nikon, Japan) with the excitation/emission wavelength at 488/525 nm, and quantified using Image J software.

### Inhibition of Nrf2 with ATRA and small inhibitor RNAs (siRNA)

Inhibition of Nrf2 was conducted using an ATRA concentration that did not significantly affect the cell viability. Briefly, cells (5×10<sup>3</sup> cells/well) were

seeded into 96-well plates and incubated for 24 h. Then the cells were treated with 5 μM ATRA for 24 h. After ATRA pretreatment, CFA treatment and following assays were conducted.

Inhibition of Nrf2 was also conducted using an Nrf2 siRNA (Santa Cruz). Briefly, cells were seeded into 6-well or 96-well plates and incubated for 24 h. Then the cells were transformed with Nrf2 siRNA for 24 h. After Nrf2 siRNA pretreatment, CFA treatment and following assays were conducted as above.

### Mitochondrial labeling and confocal microscopic observation

The SH-SY5Y cells were grown on 35-mm<sup>2</sup> confocal dishes (Axygen, USA). After treatment with 10 or 100 μM CFA for 36 h, the cells were incubated with 50 nM MitoTracker Red CMXRos for 10 min at 37 °C. Then the cells were washed three times with FBS-free DMEM medium and observed on a confocal laser scanning microscope (Nikon, Japan) with the excitation/emission wavelength at 579/599 nm. The length of mitochondrial in SH-SY5Y cells was analyzed by an Image J software.

### Determination of intracellular ATP level

The ATP level in SH-SY5Y cells was determined using an ATP bioluminescence assay kit (Beyotime). Briefly, The SH-SY5Y cells were grown on 6-well culture dishes. After CFA (100 μM) treatment, the cells were harvested and lysed with a lysis buffer, followed by centrifugation at 10,000 ×g for 2 min at 4°C. Finally, the level of ATP was determined by mixing 50 μL of the supernatant with equal volume of luciferase reagent, which catalyzed the light production from ATP and luciferin. The emitted light was linearly related to the ATP concentration and measured using a microplate Luminometer (Centro XS<sup>3</sup> LB 960).

### Measurement of oxygen consumption rate (OCR) and extracellular acidification rate (ECAR)

The mitochondrial OXPHOS function and glycolysis capacity of SH-SY5Y cells were measured by determining the oxygen consumption rate (OCR) and extracellular acidification rate (ECAR), respectively, with a Seahorse XF24 extracellular flux analyzer (USA) [33]. SH-SY5Y cells were seeded at 4×10<sup>4</sup>/well and incubated overnight and applied to Seahorse analyzer. Each analysis was conducted in three replicates.

For measuring OCR with intact cells, the experiment was performed in medium consisting of 25 mM glucose, 2 mM sodium pyruvate in unbuffered DMEM, pH 7.4, at 37 °C. The OCR values (pmol/min)

were monitored during sequential addition of Oligomycin A (OM; an ATP synthase inhibitor; final concentration, 1  $\mu\text{M}$ ), carbonylcyanide *m*-chlorophenylhydrazone (FCCP; a mitochondrial uncoupler; final concentration, 500 nM), antimycin A (AA; complex III inhibitor; final concentration, 1  $\mu\text{M}$ ) and rotenone (Rot; complex I inhibitor; final concentration, 1  $\mu\text{M}$ ) according to the OCR testing protocol.

For measuring ECAR, the experiments were performed in unbuffered DMEM, pH 7.4, at 37 °C. The ECAR values (mpH/min) were monitored during sequential addition of glucose (final concentration, 10 mM), Oligomycin A (final concentration, 1  $\mu\text{M}$ ), and 2-deoxyglucose (2-DG; inhibitor of glycolysis; final concentration, 100 mM) according to the ECAR testing program.

### Primary neuron culture

Culture plates were prepared by coating with poly-D-lysine (40  $\mu\text{g}/\text{ml}$ ) incubating at 37 °C /5%  $\text{CO}_2$  incubator overnight. The dishes/coverslips were washed three times with sterile water 1-2 hours before beginning the dissection. C57 neonatal mice were prepared by disinfecting their skin with 75% alcohol, removing the whole brain and placing in a 10 cm dish with cold dissection media (50 ml Neurobasal A, 1 ml B-27, 125  $\mu\text{l}$  glutamine). After removal of the meninges and blood vessels under the dissecting microscope, the cortical/hippocampal region was dissected and placed in new cold dissection media. Dissection media was replaced with room temperature (RT) dissection media and incubated at 30 °C for 8 min. Tissue was transferred to enzyme solution (12 ml DMEM, 30  $\mu\text{l}$  glutamine, 48  $\mu\text{l}$  DNase, 216  $\mu\text{l}$  papain) and incubated at 30 °C for 15 min. Afterwards, tissue was washed with culture media (DMEM 45 ml, FBS 5 ml and 0.5 ml penicillin/streptomycin) three times before two rounds of trituration in culture media. Supernatant was transferred to a new tube through a filter, and centrifuged at 1100 rpm for 5 min in a 50 ml conical tube. Cells were seeded into 96-well plates, 6-well plates and other culture plates at a density of 2.5-3 million cells/ml. Media was replaced with Neurobasal Media (47.5 ml Neurobasal A, 1ml B-27, 0.5 ml glutamine, 0.5 ml penicillin/streptomycin) on the following day, then exchanged with fresh media containing AraC at a final concentration of 5  $\mu\text{M}$ . Cells were then cultured for approximately 12 days, with a 1/2 media change every 3 days with Neurobasal Media continuing 5  $\mu\text{M}$  AraC.

Mouse primary neurons were treated with 100  $\mu\text{M}$  CFA for 36 h with or without  $\text{A}\beta_{42}$  (5  $\mu\text{M}$ ) stress. Cell viability was evaluated by MTS assay.

Immunofluorescence in primary cultured neurons under CFA protection was visualized with FITC-labeled MAP2 antibodies (green) and Hoechst (blue) on a confocal laser-scanning microscope (Nikon, Japan) with the excitation/emission wavelength at 488/525 nm.

### Mice

APP<sup>swe</sup>/PS1<sup>dE9</sup> (APP/PS1) transgenic mice (male, female, SPF grade) and littermate negative C57BL/6 mice (male, SPF grade) were purchased from Model Animal Research Center of Nanjing University. The APP/PS1 mice over-express the delta exon 9 variant of presenilin 1 (PS1) in combination with the Swedish mutation of  $\beta$ -amyloid precursor (APP). The mice were maintained and handled with the approval of Institutional Review Board for Laboratory Animal Care (Approval No. LA2015054), and fed in a barrier environment in Department of Laboratory Animal Science, Peking University Health Science Center.

Mice were allocated randomly into four groups as follows: (I) WT (littermate negative C57BL/6 male mice) (n=8~10) as the negative control; (II) APP/PS1 (untreated mice) (n=8~10) as the positive control; (III) ineffective low dose (0.02 mmol  $\text{kg}^{-1}\text{day}^{-1}$ ) CFA-treated APP/PS1 mice (n=8~10); (IV) effective high dose (0.2 mmol  $\text{kg}^{-1}\text{day}^{-1}$ ) CFA-treated APP/PS1 mice (n=8~10). The drug administration started at 3 months of age, by feeding the animal with pellet food containing desired amounts of CFA. Throughout the experimental period, the body weight, water and food intake were monitored. The behavior evaluations including step-down passive avoidance tests and Morris water maze (MWM) experiments were performed to monitor the alteration of learning and memory ability.

### Step-down passive avoidance test

At 5 months old (2 months after drug oral administration), the learning and memory in the mice were examined by using the step-down type of passive avoidance task. The test apparatus consisted of eight chambers (12×12×18 cm) having a grid floor with a wooden platform (5×5×4.5 cm) at the right lower corner of the grid floor within a chamber illuminated with a 15 W lamp. During the experimental period, each mouse was gently placed on the grid floor with back against the platform, and electric shocks (0.25 mA) were continually delivered to the grid floor. When the mice receive electric stimulus, they find and jump up on the platform; however, the mice will jump down when they forget the electric shock. The time period for mice staying on the platform between a jump-up and jump-down was

recorded as step-down latency. The number of step-down events during the 5-min trial was counted as "errors". The first step-down latency and error are regarded as the learning latency and learning error, respectively. The tests were repeated after different retention times (24 h and 1 month), and the corresponding data were regarded as memory latency and memory error.

### Morris water maze test

The Morris water maze (MWM) task was performed at the end of the drug treatment. The maze consisted of a circular pool (150 cm in diameter, 60 cm in height) filled with water (temperature at  $22 \pm 1$  °C), which was rendered opaque by adding white food dye. The pool contained various prominent visual cues and conceptually divided into four equal quadrants (I, II, III, IV) by imaging lines. The performance of the mice was recorded with an automated tracking system during all phases of the task.

*Visual cue phase.* Following habituation, visible platform training was performed to measure motivation of the mice to find a platform, visual acuity of the mice, and the ability of mice to use local cues. On day 1-3, a platform (diameter, 10 cm), half-way between the center and the wall, was labeled with a flag and placed 1 cm above the surface of the water in the center of a quadrant. All animals entered the water facing the wall of the pool and were allowed to explore the platform for 60 s, and if they reached the visible platform, they remained there for 5 s. If they did not find the platform within 60 s, they were guided there by the experimenter and remained there for 20 s. The starting quadrant was changed to the II, III, IV quadrants respectively each day. During the visual cue phase of training, speed and latency to the platform were used to compare the performance between animal groups and screen out mice with poor eyesight.

*Acquisition phase.* On day 4-9, the last hidden platform trial was conducted to measure the ability of mice to form a representation of the spatial relationship between a safe, but invisible (submerged 1 cm below the water level) platform (10 cm in diameter) without flag and visual cues surrounding the maze. The platform was replaced in the center of IV quadrant, and several extra maze cues were distributed across the walls surrounding the pool. The starting quadrant was changed in I, II, III quadrants respectively each day. Animals were allowed 60 s to locate the platform and 5 s to rest on it. Mice that failed to find the platform were led there by the experimenter and allowed to rest there for 20 s. The acquisition time (latency to reach the platform) and

path length (distance swam to the platform) were used to analyze and compare the performance between different treatment groups.

*Probe trial phase.* Twenty-four hours following the last hidden platform trial, the probe test was carried out by removing the platform and allowing each mouse to swim freely for 60 s. All animals were placed in quadrant I, opposite the target quadrant IV (where the platform had been located during hidden platform training). The time and distance that mice spent swimming in the four quadrants and other parameters were recorded to assess the ability of the mouse to remember the previous location of the platform.

### Mouse brain samples

One week after the Morris water maze (MWM) task, all of the animals were weighed and euthanized. The brain was immediately harvested and separated sagittally in two hemispheres. One hemibrain was fixed overnight by immersion in 10% buffered formalin at RT and embedded in paraffin. The other hemibrain was dissected on ice to obtain hippocampus, frontal lobe, and cerebellum, and samples were stored at -80 °C for further analysis.

### Human brain samples

Sections of cortex were obtained from the brains of healthy aged control and Alzheimer's disease patients at autopsy following protocols approved by the University of Washington School of Medicine. In all cases where AD was diagnosed at autopsy, AD was stated as the cause of death. AD subjects had no evidence of other neurological disease based on neuropathological examination.

### Brain histology and immunohistochemistry

The 5-mm-thick paraffin sections of hemibrain were prepared for haematoxylin-eosin (HE) staining, Nissl staining and amyloid- $\beta$  (A $\beta$ ) immunohistochemistry. Quantitative analysis of surviving cells was performed at 40 $\times$  magnification (Olympus BX51, JAPAN). The total number of neurons without basophilic lesions in the dentate gyrus, as well as the total number of neurons and basophilic cells in combined CA1-4, were counted in HE pathological sections. Mean values were calculated from 5-6 fields in three levels with HE pathological sections per animal in each region. Immunostaining of A $\beta$  forms was performed using a 6E10 antibody (1 : 200; BioLegend) by overnight incubation at 4 °C. The HRP-conjugated secondary antibody was then incubated for 1 h at room temperature. The images were visualized finally with DAB (3,3-diaminobenzidine), paying special attention to the hippocampus, cerebral cortex and cerebellum.

The Nrf2 immunohistochemistry was conducted the same as above.

### Brain tissue sequential extraction

All extractions were performed on ice or at 4 °C. Weighed samples of hippocampus, cerebral cortex and cerebellum tissues were added to 10 times the mass of pre-chilled Tris buffer (1 mM Tris, 1 mM EGTA, 1 mM DTT, 10% sucrose, pH 7.5) and homogenized with a bullet blender (Gene Company Limited, Hong Kong). Then homogenates were centrifuged at 26,000×g for 15 min. The supernatant (**water soluble fraction**) was then collected and stored at -80°C. The pellet was re-suspend in pre-chilled 1% Triton X-100 solution containing 1 mM Tris-HCl (pH 7.5), 1 mM EGTA, 1 mM DTT, and 10% sucrose. Then, the sample was centrifuged at 23,000×g for 1 h. The supernatant (**water insoluble/lipid soluble fraction**) was collected and stored at -80°C.

### Preparation of Eu-DTPA-A $\beta$

Eu-DTPA-A $\beta$  was prepared according to the previous method [34]. Briefly, the DTPA-A $\beta$  conjugates were prepared by adding 0.18 mg of DTPAA dissolved in DMSO to A $\beta$  (1 mg) solution in 1ml 0.05 M carbonate buffer solution (pH 8-10) under vigorous stirring. The coupling reaction proceeded 3-4 h at r.t. in order to make A $\beta$  react completely [35]. Then, the reaction solution was dialyzed (cut off 1kDa) by phosphate buffered solution (pH 7.0) to remove the unreacted DTPAA. Then, 0.01M EuCl<sub>3</sub> was added dropwise until appearance of a white sediment to prepare the Eu-DTPA-A $\beta$ . After centrifugation (3 min, 10000×g), the supernatant (Eu-DTPA-A $\beta$ ) was collected and applied to a PD-10 desalting column (GE Health Care, USA), which was pre-balanced with HBSS (pH 7.0). The elute was concentrated by centrifugal ultrafiltration (Amicon Ultra-4, cut off 3 kDa). The amount of A $\beta$  was measured with enhanced BCA protein assay kit. The bound Eu was measured by time-resolved fluorescence as described in the previous method (fluorescent parameter:  $\lambda_{ex/em}$  340/616 nm; measurement window, 600-1000  $\mu$ s).

### Intrastriate Eu-DTPA-A $\beta$ injection.

APP<sup>swe</sup>/PS1<sup>dE9</sup> (APP/PS1) transgenic mice (male, SPF grade) and littermate negative C57BL/6 mice (male, SPF grade) were purchased from Model Animal Research Center of Nanjing University. Mice were allocated randomly into three groups as follows: (I) WT (littermate negative C57BL/6 male mice) (n=4~6) as the negative control; (II) APP/PS1 (untreated mice) (n=4~6) as the positive control; (III) CFA-treated APP/PS1 mice (0.2 mmol kg<sup>-1</sup>day<sup>-1</sup>) (n=4~6). The drug administration started at 5 months

of age, by feeding the animal with pellet food containing desired amounts of CFA. 2-3 weeks after drug oral administration, the A $\beta$  brain clearance experiments in the mice were conducted.

Anesthetized mice were fixed in a stereotaxic frame and body temperature was kept at 37 °C with a temperature-controlled warming pad. A 30 GA needle was inserted *via* a small burr hole into the brain at the following coordinates: intra-striate injections (0.22 mm caudal, 2.5 mm lateral, 3.5 mm ventral to bregma). After needle insertion, 30 minutes was allowed to elapse to allow the needle track to swell closed. 2.0  $\mu$ l of Eu-DTPA-A $\beta$  (dissolved in artificial CSF) was injected at a rate of 0.2  $\mu$ l/min with a syringe pump (Harvard Apparatus).

After 15, 30 or 60 minutes, animals were rapidly decapitated and the blood was collected, then the skull opened, the dura removed and the brain harvested. The brain was solublized and ground in H<sub>2</sub>O at 4 °C. Brain fluorescence was normalized to total fluorescence detected in a 2  $\mu$ l Eu-DTPA-A $\beta$  put directly into a fresh brain to grinder and expressed as the % of total injected fluorescence. Eu-DTPA-A $\beta$  clearance from the brain and accumulation in the blood was compared by two-way ANOVA.

The EVs were extracted by XYCQ EV Enrichment KIT. And the bound Eu was measured by time-resolved fluorescence as described in the previous method.

### Intracisternal FITC-A $\beta$ injection and *in vivo* fluorescence imaging

A craniotomy (2×2 mm in diameter) was made over the cortex of the anesthetized mice. The dura was left intact and the craniotomy was covered with ACSF and sealed with a glass coverslip. Then anesthetized mice were fixed in a stereotaxic frame and a 30 GA needle was inserted into the cisterna magna. 2  $\mu$ l of CSF FITC-A $\beta$  tracer was injected at a rate of 0.2  $\mu$ l/min over 10 minutes with a syringe pump (Harvard Apparatus). To visualize the vasculature, 0.1ml BBB impermeable Cy5-dextran 70 (MW 70 kD; both 1% in saline, Nanocs) was injected intra-arterially immediately before imaging. A 20× (0.9 NA) water immersion lens was used to image the cortex, from the surface to a depth of ~240  $\mu$ m. The cerebral vasculature was first imaged with 512×512 pixel frames from the surface to a depth of 240  $\mu$ m with 3  $\mu$ m z-steps. After intracisternal injection of CSF tracer, tracer movement into the cortex was conducted with dual-channel (FITC and Cy5) 512×512 pixel image acquisition.

### Western blotting

The tissue samples were prepared as described above. The cell samples were washed twice with

ice-cold phosphate buffer solution (PBS) and lysed on ice with pre-cooled RIPA lysis buffer containing protease and phosphatase inhibitor cocktails. The samples were centrifuged at 12,000×g for 20 min at 4°C. The supernatant was collected.

The total protein levels of the samples were determined with a BCA protein quantitation kit. Aliquots containing 25 µg total protein were applied to SDS-PAGE gel separation. Then, the protein bands were transferred to polyvinylidene fluoride (PVDF, Millipore) membranes. After blocking with 5% nonfat dry milk or 5% (Bovine Serum Albumin) BSA for 2 h, membranes were incubated with desired primary antibodies (Aβ, Nrf2, HO-1, Drp1, PKM2, p-Tau, p-GSK-3β, p-AKT or GAPDH) overnight at 4°C and then secondary antibody for another 1h at room temperature. After washes, the protein bands were visualized with an ECL Western blotting substrate kit and observed on a chemi-luminescence imaging system. The protein bands were quantified using ImageJ software (National Institutes of Health, USA).

### Statistical analysis

Data were expressed as mean±standard deviation (SD) or mean±standard Error of Mean (SE). Differences between groups were analyzed by two-way analysis of variance (ANOVA) and  $P < 0.05$  was considered as statistically significant. Statistical analyses were carried out using Origin 8.0 or SPSS.

## Results

### Coniferaldehyde promotes neural cell viability and protects cells from Aβ stress and mitochondrial toxins.

We screened a variety of cinnamaldehyde derivatives including *o* or *m* or *p*-hydroxycinnamaldehyde, *o* or *m* or *p*-methoxycinnamaldehydes, ferulaldehyde, sinapaldehyde, and 4-hydroxy-3-methoxycinnamaldehyde (coniferaldehyde, CFA) in three SH-SY5Y cellular models stably transformed with a control vector (neo), a vector expressing amyloid precursor wild type protein (APPwt), or a vector expressing APP protein with the Swedish mutation (APPswe), respectively. Among the tested compounds, CFA best promoted cell growth in all three cellular models. The effects were significant within the range of 30~160 µM, with maximal promotion at 80~100 µM (Fig. 1B). It is noted that CFA treatment significantly up-regulated the level of brain-derived neurotrophic factor (BDNF) (Fig. S1), suggesting the possible involvement of neurotrophic signaling pathways in the actions of CFA.

Because cinnamaldehyde has previously demonstrated mitochondrial protection against

oxidative stress [30], the ability of CFA to reduce damage induced by the mitochondrial-targeting agents MPP<sup>+</sup> (1-methyl-4-phenylpyridinium) and rotenone (Rot) was examined. CFA (50 µM) effectively alleviated the neuronal cell damage (Fig. 1C-D) caused by MPP<sup>+</sup> or Rot. Even 10 µM CFA significantly reduced SH-SY5Y cell death induced by MPP<sup>+</sup> treatment (Fig. 1C). These results indicate that CFA protects neural cells, likely *via* mitochondria.

To further characterize the neuroprotection by CFA, primary cultured neurons were stressed by exposure to 5 µM Aβ<sub>42</sub> and then treated with 100 µM CFA. Neurons exposed to Aβ<sub>42</sub> demonstrated morphological disruption including reduction of axon outgrowth and decreased neurite elaboration (Fig. 1E-F). Remarkably, CFA treatment significantly preserved the normal morphology of primary neurons (Fig. 1E) and improved cell viability (Fig. 1F) in both the absence and presence of Aβ<sub>42</sub>. All the results above indicated that CFA is an excellent neuroprotective agent.

### The role of Nrf2 signaling in the protective effect of coniferaldehyde.

We next sought to confirm that CFA protects neurons through activation of the Nrf2 pathway, as hypothesized based on our screening process. Under the resting state, Nrf2 is sequestered in the cytoplasm by its binding partner, Kelch-like ECH-associated protein 1 (Keap1) [21-24, 36, 37]. Upon activation, it is translocated to the nucleus, where it activates its downstream targets. Therefore, we investigated the localization of Nrf2 following CFA treatment. As expected, CFA treatment significantly promoted the translocation of Nrf2 from the cytosol to the nucleus (Fig. 2A-D and S2). While Nrf2 levels were lower in Aβ-overexpressing cells (APPwt and APPswe) (Fig. S3) than in SH-SY5Y neo cells, CFA treatment dose-dependently increased Nrf2 expression in all three cell lines (Fig. 2E-F and S3) as well as up-regulated the expression of HO-1 (Fig. 2G-H and S3), a major downstream target of Nrf2 activation [38]. Overall, this evidence demonstrates activation of Nrf2 by CFA *in vitro*.

To further demonstrate whether the neuroprotective and survival-enhancing effects of CFA are mediated by Nrf2 activation, the cells were pretreated with Nrf2 siRNA to knock down expression [39] or all-trans-retinoic acid (ATRA) to block Nrf2 signaling [40]. The conditions for Nrf2 knockdown were carefully selected to reduce Nrf2 levels (Fig. S4) without significantly affecting the cell viability. The results (Fig. 2I) showed that Nrf2 knockdown mostly diminished CFA-induced increase of cell viability (by 60~80%) in the three SH-SY5Y

cells. Similarly, inhibition of Nrf2 signaling with ATRA also largely reduced CFA-induced increase in cell viability (by 60~70%) in the SH-SY5Y cells (Fig. 2J) and abolished HO-1 expression by CFA (Fig. 2G-H). All these results indicated Nrf2 activation is responsible for most neuroprotective effects of CFA against A $\beta$  toxicity.

### Coniferaldehyde protects mitochondrial structure and function in SH-SY5Y cells with A $\beta$ burden.

A $\beta$ -induced mitochondrial dysfunction has been shown to be tightly linked to AD development and progression [18, 19, 41]. The mitochondrial dysfunction is mainly a shift of mitochondrial dynamics towards fission [42-44] and of energy metabolism from primarily driven by oxidative

phosphorylation towards glycolysis (similar to the Warburg effect [45, 46] in cancer). Therefore, we tested the effects of CFA on mitochondrial structure and function in SH-SY5Y cells.

First, we examined the effect of CFA on mitochondrial morphology. As shown in Fig. 3A, mitochondria in the SH-SY5Yneo cells had normal, threadlike shapes. However, most mitochondria in the APP<sup>swe</sup> cells were swollen and oval-shaped, with an intermediate phenotype in APP<sup>wt</sup> cells. Upon treatment with CFA (100  $\mu$ M), most mitochondria in the APP<sup>swe</sup> cells regained normal thread-like morphology. To our best knowledge, CFA is the first agent that could reverse the mitochondria fission (Fig. 3A-B) induced by A $\beta$  burden.

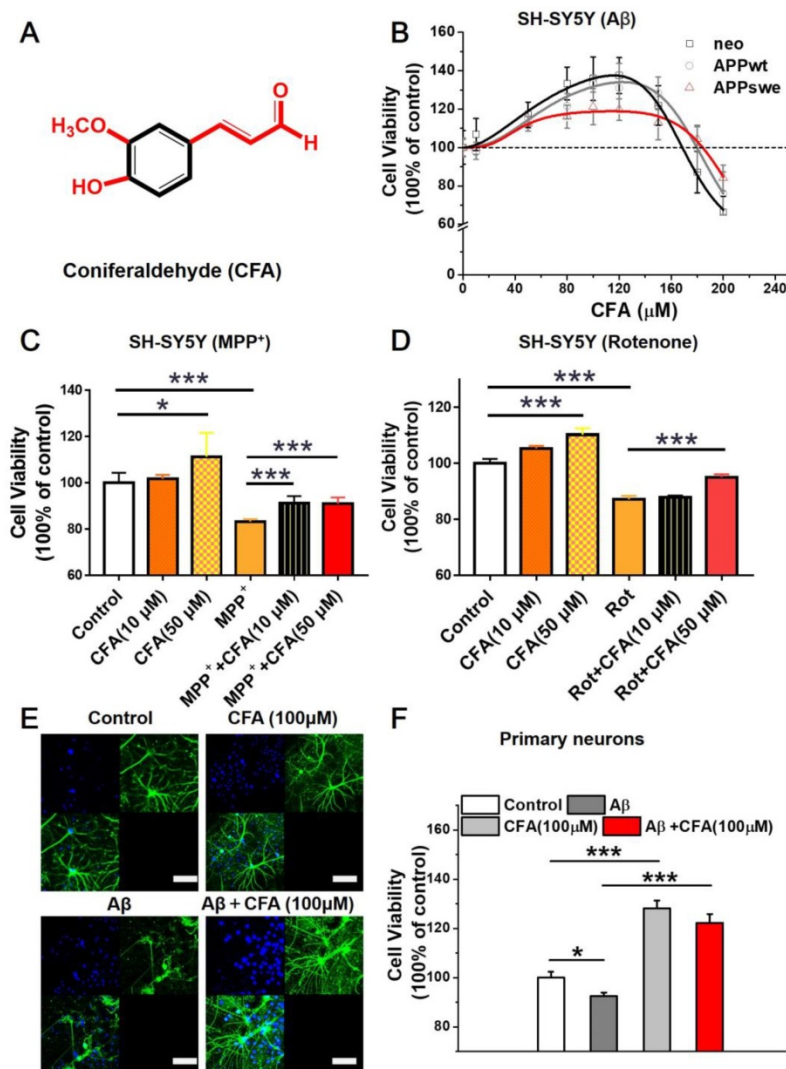


**Figure 1. CFA improved neuronal cell viability and protected cells against A $\beta$  stress and mitochondrial toxins. (A)** Chemical structure of CFA. **(B)** The effects of coniferaldehyde (CFA) on the viability of SH-SY5Y cells (neo, APP<sup>wt</sup> and APP<sup>swe</sup>) with/without A $\beta$  burden, 300  $\mu$ M MPP<sup>+</sup> (1-methyl-4-phenylpyridinium) **(C)** or 1  $\mu$ M rotenone (Rot) **(D)** 24 h pre-induced SH-SY5Y cells. All kinds of cells were treated with CFA for 36 h before quantification of cell viability by MTS assay. **(E)** Representative immunofluorescence images of CFA-treated and control primary cultured neurons. Mouse primary neurons were treated with 100  $\mu$ M CFA for 36 h with or without A $\beta$ 42 (5  $\mu$ M) stress. The neurons were visualized with FITC-labeled Microtubule Associated Protein 2 (MAP2) antibodies (green) and Hoechst (blue). Scale bars, 75  $\mu$ m. **(F)** Improvement of cell viability upon CFA treatment with/without A $\beta$ 42 (5  $\mu$ M) stress in primary cultured neurons. Results are mean $\pm$ SD (n=3). \*P<0.05, \*\*\*P<0.001 versus control or specific indication.

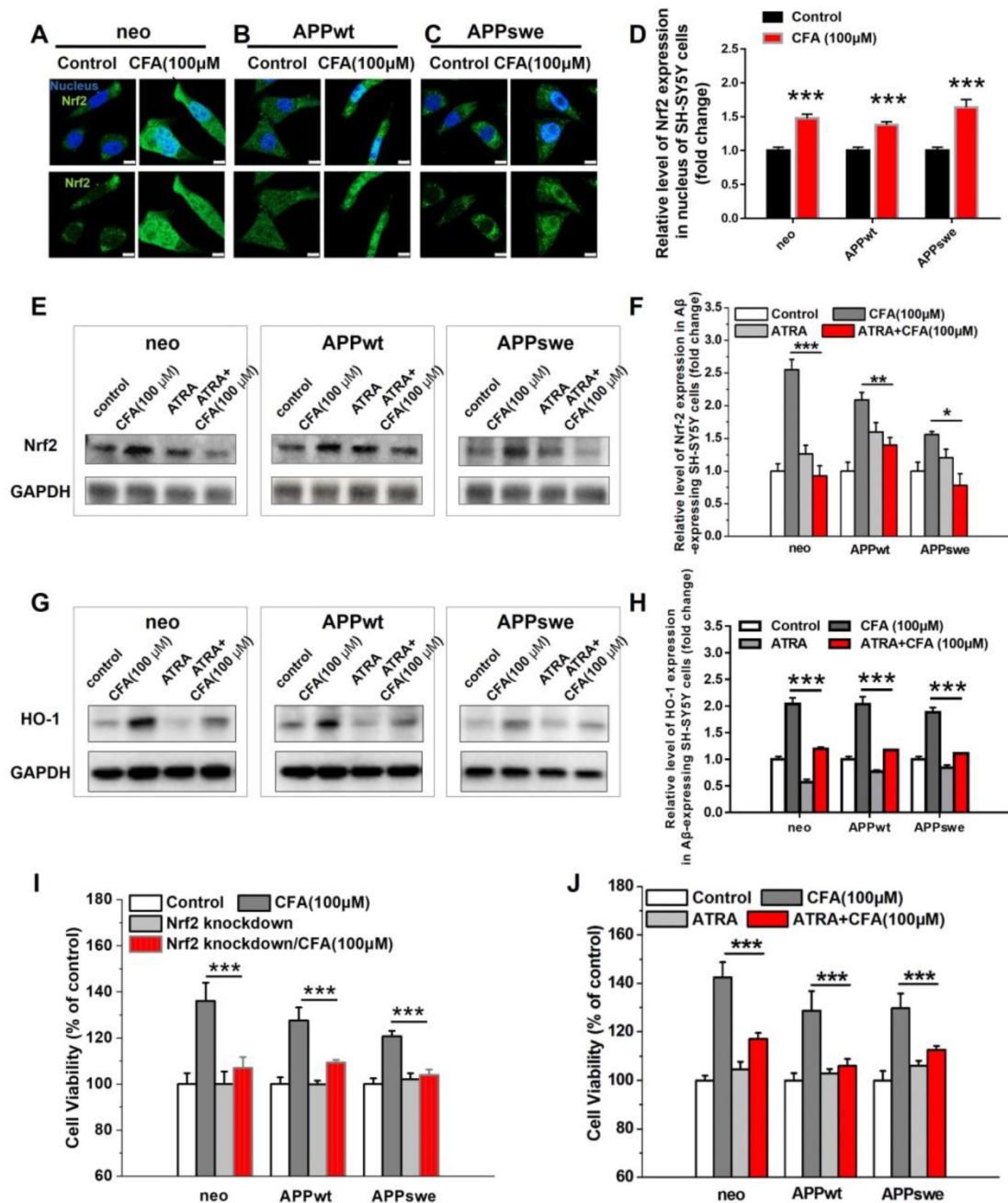


**Figure 2. CFA treatment activated Nrf2 in SH-SY5Y cells with & without A $\beta$  burden responsible for most neuronal protective effects. (A–C)** Representative immunofluorescence image of Nrf2 (green) translocation into nucleus (blue) upon treatment of A $\beta$ -expressing SH-SY5Y (neo, APPwt and APPswe) cells with 100  $\mu$ M CFA. Scale bars, 10  $\mu$ m. **(D)** Quantification of nuclear vs cytoplasmic Nrf2 expression based on the imaging (A–C). **(E–H)** Nrf2 expression **(E,F)** and HO-1 expression **(G,H)** were elevated upon CFA treatment (100  $\mu$ M) but inhibited by pretreatment with all-trans-retinoic acid (ATRA, 5  $\mu$ M, 24 h); **(I)** Nrf2 knockdown with siRNA significantly decreased improvement of cell viability by CFA (100  $\mu$ M). **(J)** ATRA treatment significantly decreased improvement of cell viability by CFA (100  $\mu$ M). Results are mean $\pm$ SE (n=3). \*P<0.05, \*\*P<0.01, \*\*\*P<0.001 versus CFA group.

Next, we investigated the effect of CFA treatment on ATP production in all three cells using a bioluminescence-based assay, and found that CFA treatment significantly increased it in all three cell lines (Fig. 3C). We further measured the contribution of the two major aspects of mitochondrial ATP production [47], i.e. oxidative phosphorylation and glycolysis, on a Seahorse XF Extracellular Flux Analyzer. In the tests of oxygen consumption rate (OCR), a measure of oxidative phosphorylation (Fig.

3D), CFA increased the basal and maximal respiration rates mostly without affecting the coupled respiration (Fig. 3E–G). In contrast, the extracellular acidification rate (ECAR) (Fig. 3H), largely a measure of glycolysis, was decreased by CFA, suggesting decrease of glycolysis in the three SH-SY5Y cells (Fig. 3I–K). Together, these results indicated that CFA significantly promoted the pattern of ATP production towards oxidative phosphorylation, i.e. improved mitochondrial function.

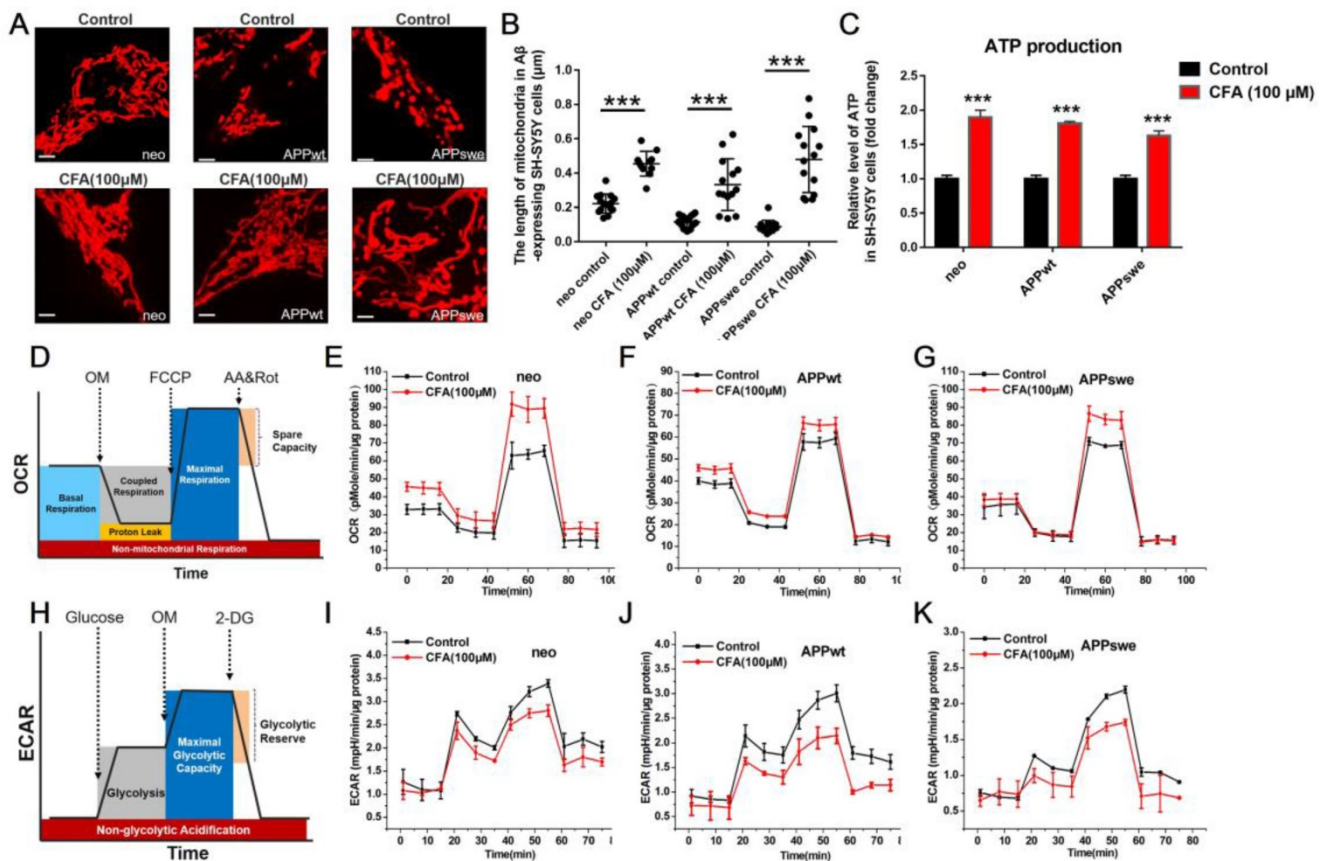


**Figure 3.** CFA treatment improved the mitochondrial morphology and energy production in A $\beta$ -expressing SH-SY5Y cells. (A–B) Morphological changes of mitochondria in SH-SY5Y cells with/without A $\beta$  burden upon CFA treatment. SH-SY5Y cells (neo, APPwt and APPsw) were treated with 100  $\mu$ M CFA and mitochondria were stained with MitoTracker Red CMXRos. Scale bars, 2.5  $\mu$ m. (C) Substantial increase in ATP production by CFA treatment. (D–K) Enhancement of mitochondrial aerobic respiration/oxidative phosphorylation by CFA. D,H: illustration of oxygen consumption rate (OCR) and extracellular acidification rate (ECAR) measurement on a Seahorse XF Extracellular Flux Analyzer, in which oligomycin (OM) inhibits ATP synthase to block coupled respiration, FCCP serves as a mitochondrial uncoupler to resume oxygen consumption, AA (a complex III inhibitor) and Rot (complex I inhibitor) halt oxidative phosphorylation, and 2-deoxyglucose (2-DG) inhibits hexokinase to stop glycolysis. As Figure 3H–K showed, CFA stimulated a slight decrease in ECAR over basal glycolysis, but result in an obvious decrease in maximum glycolytic capacity; E–G: The OCR of A $\beta$ -expressing SH-SY5Y cells upon 100  $\mu$ M CFA treatment; I–K: The ECAR of A $\beta$ -expressing SH-SY5Y cells upon 100  $\mu$ M CFA treatment. Each experimental group was analyzed using three replicates in each analysis. Results are mean $\pm$ SD ( $n=3$ ).

We next explored the effect of CFA on the key proteins regulating mitochondrial structure and function. First, we measured CFA-induced changes on Drp1, a member of the family of large GTPases that stimulates fission when recruited to the mitochondrial membrane [43, 48, 49]. As shown in Fig. 4, CFA treatment caused a dose-dependent decrease in Drp1 expression in all SH-SY5Y cell lines (Fig. 4A–B) albeit less significantly in APPsw cells, where the A $\beta$  burden in the highest. Similarly, CFA treatment also reduced Drp1 level in primary cultured neurons under A $\beta$  stress (Fig. 4E–F) and membrane-associated Drp1 in brain of APP/PS1 mice (Fig. S5). Next, we sought to determine the effect of CFA on pyruvate kinase isoform 2 (PKM2), which catalyzes the rate-limiting step of glycolysis and is crucial for the Warburg effect [45, 46]. CFA dose-dependently down-regulated PKM2 expression in SH-SY5Y cells (Fig. 4C–D) or abolished A $\beta$ -induced PKM2 elevation in primary cultured neurons (Fig. 4G–H). Together with the improvement of mitochondrial oxidative

phosphorylation shown in Fig. 3 above, this finding is consistent with a restoration of normal energy production and a reversal of the A $\beta$ -induced shift toward glycolysis.

In addition, CFA (100  $\mu$ M) treatment ameliorated dysfunction of mitochondrial membrane potential ( $\Delta\Psi_m$ ) and reactive oxygen species (ROS) production in APPwt and APPsw cells (Fig. S6 and S7). All these results are consistent with a reversal of A $\beta$ -induced shift of mitochondrial energy metabolism.

### The potential effects of CFA on Tau pathology

In AD pathogenesis, there is crosstalk between A $\beta$  toxicity and intracellular neurofibrillary tangles (NFTs), another histological hallmark of AD [50, 51], which are composed of hyperphosphorylated microtubule associated protein Tau [50, 51]. We observed a dose-dependent decrease of p-Tau (S262) (Fig. 5A–B) and p-Tau (S422) (Fig. 5C–D) in A $\beta$ -expressing cells upon CFA treatment. The precise mechanism underlying this phenomenon remains to

be investigated; but it is possible that improved mitochondrial energy metabolism increases the phosphorylation-dependent activation of Akt/PKB (Fig. 5E-F) and subsequent phosphorylation inactivation of glycogen synthase kinase-3 $\beta$  (GSK-3 $\beta$ , a major kinase for Tau [52]) (Fig. 5G-H). It is also possible that increased A $\beta$  transport (see below for more results and discussion) attenuated A $\beta$ -tau cascade, as proposed by others.

### Coniferaldehyde treatment re-activates Nrf2 in APP/PS1 mice

In AD patients, Nrf2 was found in the inactive state as indicated by retention of Nrf2 in the cytosol [25, 26]. Upon histological analysis of Nrf2 subcellular localization in brains of AD patients obtained at autopsy, we found that the level of nuclear Nrf2 was significantly lower than that of normal elderly controls (Fig. 6A-C). Consistently, a similar pattern of Nrf2 subcellular localization was observed in APP/PS1 AD model mice *versus* WT control (Fig. 6D-G), suggesting chronic A $\beta$  toxicity may be one major reason for Nrf2 inactivation. Not surprisingly, CFA treatment up-regulated Nrf2 expression in a dose-dependent manner (Fig. 6H-I) and particularly, CFA(H) (high dose, 0.2 mmol kg<sup>-1</sup>d<sup>-1</sup>) dramatically

reversed the nuclear localization of Nrf2 (Fig. 6F-G), indicating the recovery of Nrf2 activity.

### Coniferaldehyde enhanced brain A $\beta$ excretion via both free and extracellular vesicle-bound forms in APP/PS1 AD mice.

Nrf2 has a role in facilitating drug/metabolic waste excretion [21-24, 36, 37]. Therefore, we also tested whether CFA affected brain A $\beta$  excretion *in vivo* in APP/PS1 transgenic mice, a well-recognized AD animal model [53]. As shown in Fig. 7A-B, after intrastriatal injection [54] of A $\beta$ <sub>42</sub> labeled with a fluorescent lanthanide (i.e. Eu<sup>3+</sup>) complex, the brain content of fluorescent A $\beta$  was observed to decrease rapidly with time. Data fitting to a model of one exponential decay ( $y = Ae^{-x/t} + y_0$ ) showed that the retention time constants ( $t$ ) and maximal excretion of A $\beta$  ( $A$ ) in brain were  $0.19 \pm 0.02$  h and  $53 \pm 1\%$  for WT mice,  $0.23 \pm 0.02$  h and  $61 \pm 1\%$  for APP/PS1 mice, and  $0.14 \pm 0.02$  h and  $64 \pm 2\%$  for CFA(H)-treated APP/PS1 mice, respectively. Meanwhile, the levels of A $\beta$  in peripheral blood were observed to increase reciprocally to the decrease of brain A $\beta$  (Fig. 7C). Data fitting to a model of one exponential growth ( $y = y_0 + A(1 - e^{-x/t})$ ) presented that the time constants ( $t$ ) and relative amounts of plasma A $\beta$  ( $A$ ) were  $0.19 \pm 0.02$  h

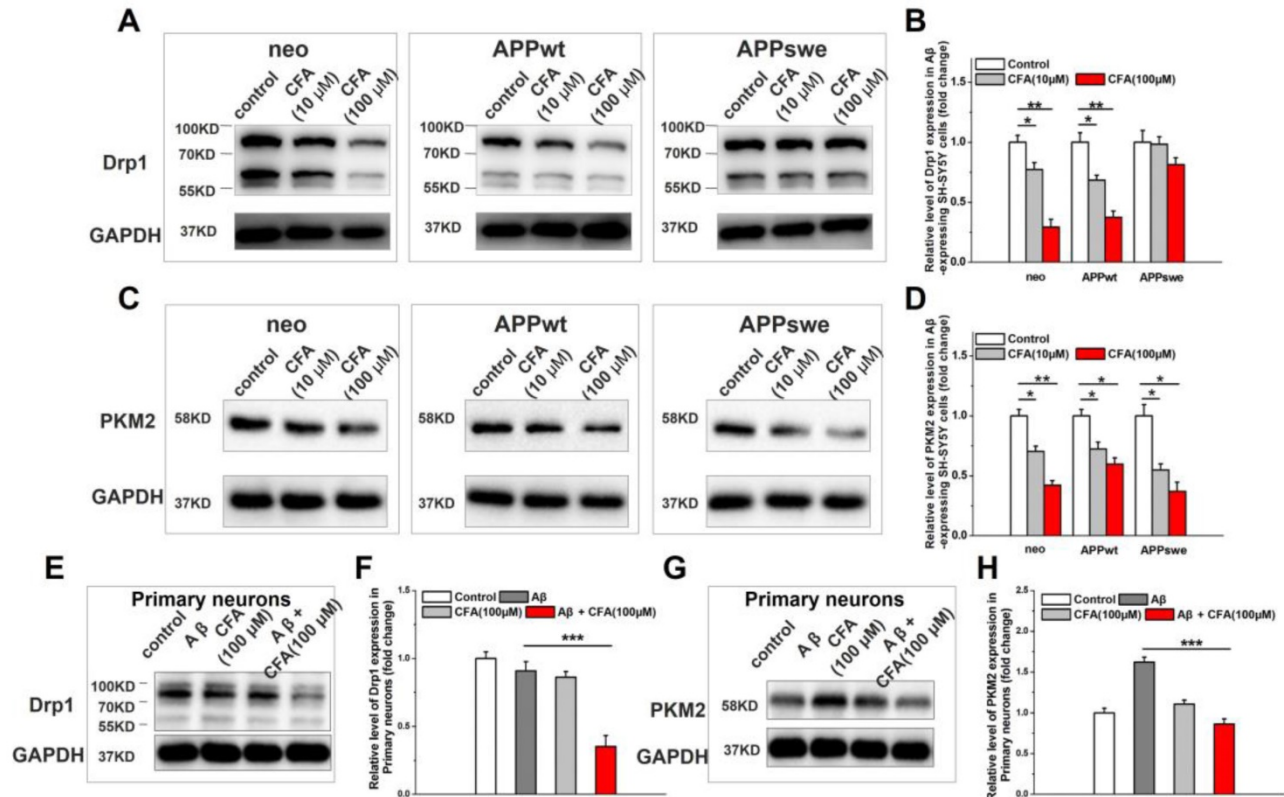


**Figure 4.** The effect of CFA treatment on Drp1 expression and PKM2 expression on A $\beta$ -expressing SH-SY5Y cells and primary cultured neurons upon A $\beta$ <sub>42</sub> treatment. SH-SY5Y cells (neo, APPwt and APPswe) were treated with 100  $\mu$ M CFA and the levels of Drp1 (A,B) and PKM2 (C,D) were analyzed by western blot. \* $P < 0.05$ , \*\* $P < 0.01$  versus control. Primary cultured neurons were treated with 100  $\mu$ M CFA in presence/absence of 5  $\mu$ M of A $\beta$ <sub>42</sub> for 36 h, Drp1 (E,F) and PKM2 (G,H) levels were analyzed by western blot. Results are mean  $\pm$  SE ( $n = 3$ ). \*\*\* $P < 0.001$  versus A $\beta$  group.

and  $22.3 \pm 0.2$  (WT mice),  $0.20 \pm 0.02$  h and  $23.5 \pm 0.4$  (untreated APP/PS1 mice),  $0.17 \pm 0.02$  h and  $33.3 \pm 0.6$  (CFA-treated AD mice,  $P < 0.1$  vs WT or APP/PS1), respectively. The results of decreased A $\beta$  and increased plasma A $\beta$  levels are in good agreement with each other. Overall, these results showed that CFA treatment significantly increased the rate and amount of brain A $\beta$  clearance by 30~40% ( $P < 0.01$  vs WT or APP/PS1 mice).

To further investigate the potential pathways, we observed the A $\beta$  flux in the brain parenchyma upon intracisternal injection of FITC-labeled A $\beta$  using a two-photon laser scanning microscopy. A blood-brain barrier (BBB)-impermeable dye (Cy5-d70, intravenous injection) was used to visualize the cerebral vasculature (Fig. 7D). It was observed that labeled A $\beta$  moved along the space outside the cortical surface blood vessel (Fig. 7E-G). It is noted that A $\beta$  was viewed close to the vascular wall (Fig. 7G). Co-localization tests with intracisternal injection of both Alexa 647-labeled CD63 antibody (for staining

the extracellular vesicles (EVs) and FITC-labeled A $\beta$  (Figure 7H) revealed that the some A $\beta$  particles overlapped very well with EVs, suggesting EVs as an A $\beta$ -carrier in the process of A $\beta$  excretion.

Next, the role of EVs in A $\beta$  transport was investigated by measuring the distribution of A $\beta$  between EVs and supernatant of plasma samples. The results (Fig. 7I) showed that A $\beta$  is excreted from the brain in both EVs-bound and unbound forms. The ratio of unbound to EV-bound forms is about 54%:46% for WT control, 56%:44% for APP/PS1 mice, and 60%:40% for CFA-treated mice; and the ratios were not changed greatly with time. Therefore, about half of A $\beta$  excretes from brain to blood in EV-bound forms. CFA treatment increased A $\beta$  excretion in both pathways, albeit more enhancement for the unbound A $\beta$  form. To our best knowledge, it is the first demonstration that EVs might participate in brain A $\beta$  excretion and consistent with previous work showing that cellular A $\beta$  release may be associated with exosomes [55].

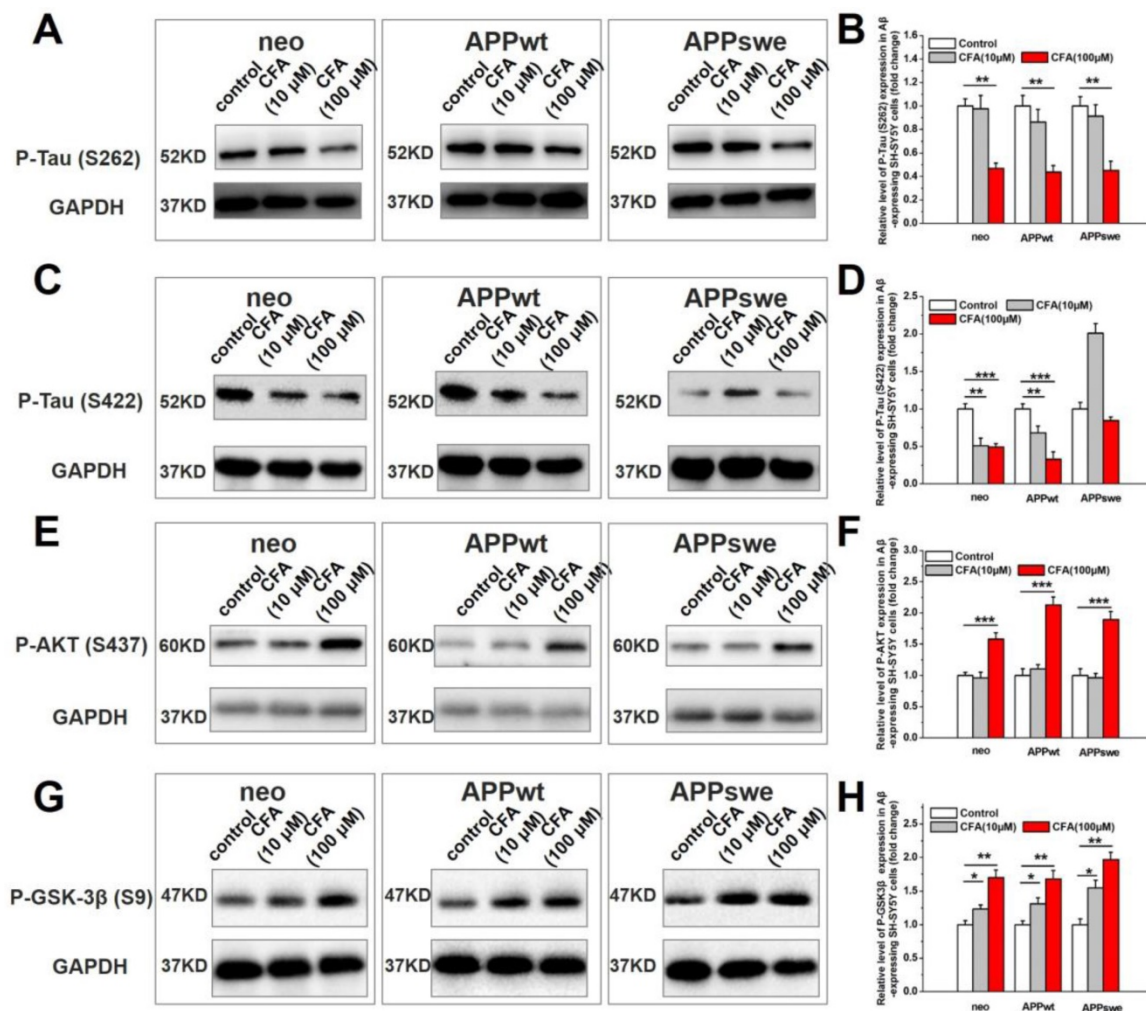


**Figure 5.** The effect of CFA on Tau phosphorylation in SH-SY5Y cells. Western blot analysis of phosphorylation of Tau (S262) (A,B), Tau (S422) (C,D), Akt (S437) (E,F), GSK-3 $\beta$  (S9) (G,H). Results are mean $\pm$ SE ( $n=3$ ). \* $P < 0.05$ , \*\* $P < 0.01$ , \*\*\* $P < 0.001$ .

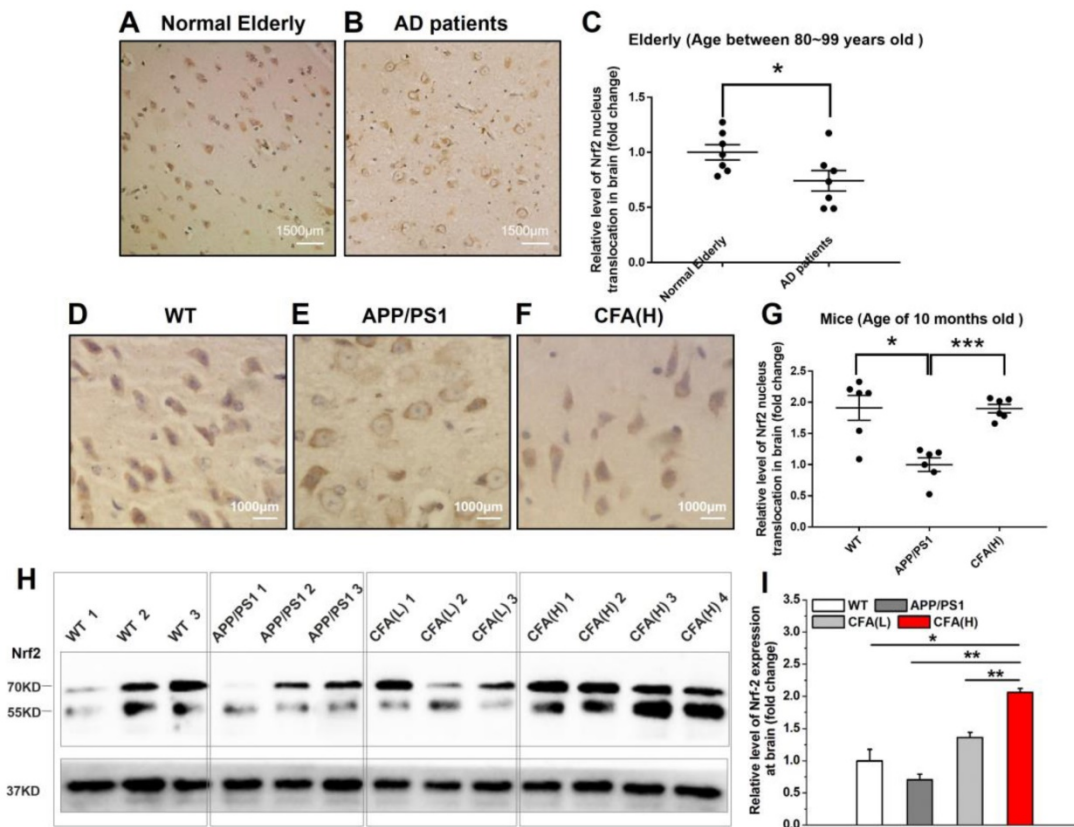


**Figure 6. CFA treatment strongly activated Nrf2 signaling in vivo.** The brain samples were immunostained with the Nrf2 antibody. (A–B) Representative images of Nrf2 staining of brain sections of Normal Elderly controls (A) and Alzheimer’s Disease patients (B). (C) Quantification of amounts of nuclear Nrf2 in (A–B). The mean age of the AD patients was  $84.7 \pm 2.1$  years, and the controls  $85.2 \pm 3.3$ . Scale bars, 1500  $\mu\text{m}$ . Results are mean  $\pm$  SE ( $n=7$ ). \* $P < 0.05$  versus Normal Elderly. (D–F) Representative images of Nrf2 staining of brain sections of WT mice (D), untreated APP/PS1 control (E) and CFA(H)-treated (F) mice. (G) Quantification of amounts of nucleus Nrf2 in (D–F). Scale bars, 1000  $\mu\text{m}$ . (H, I) Western blot of Nrf2 levels in brain of WT and APP/PS1 mice with/without CFA treatment. The mice were 10 months old and had been treated with CFA in pellet food for 7 months. Results are mean  $\pm$  SE ( $n=6$ , with random selection). \* $P < 0.05$ . Results are mean  $\pm$  SE ( $n=6$ , with random selection). \* $P < 0.05$ , \*\*\* $P < 0.001$  versus untreated APP/PS1 or specific indication.

### Coniferaldehyde preserves learning and memory function in APP/PS1 AD mice.

The ability of CFA to prevent AD-related phenotypes was tested in APP/PS1 transgenic mice. The male mice began receiving orally administered CFA at 3 months old (Fig. 8A), using two different dosing regimens, i.e. high dose, designated CFA(H) of  $0.2 \text{ mmol kg}^{-1}\text{d}^{-1}$  and low dose, designated CFA(L) of  $0.02 \text{ mmol kg}^{-1}\text{d}^{-1}$ . Learning and memory capacity was measured with two different tests, starting after 3 months of CFA treatment (i.e. at 6 months of age).

In the step-down passive avoidance test, the first trial at 6 months old (Fig. 8B–C) showed that untreated APP/PS1 mice exhibited shorter step-down latency and greater learning error than wild type (WT) mice, suggesting decreased learning capacity; however, the 24 h memory for the electric shock was preserved in untreated APP/PS1 mice (Fig. S8). Retention tests at one and two months revealed that the step down latency was significantly higher, with the step down number lower, in WT and CFA(H) treated APP/PS1 mice compared to untreated or CFA(L) treated APP/PS1 mice, indicating that CFA

treatment improved memory retention in APP/PS1 mice.

The learning and memory protection effect of CFA was further verified by the classical Morris water maze test. Theoretically, when an animal has completely lost its spatial memory, it will randomly swim, searching in the four quadrants for the hidden escape platform, while an animal that remembers the location of the platform will prefer a specific quadrant, as indicated by its staying time of  $>25\%$  within that quadrant. As shown in Fig. 8D–E, untreated and CFA(L) treated mice showed no preference for the quadrant containing the platform, while WT mice spent the greatest time in the target quadrant. Remarkably, CFA(H) treated mice demonstrated significantly increased time in the target quadrant. Moreover, CFA(H) treated mice had a significantly reduced time to the first arrival at the location of platform (Fig. 8F), and significantly increased times across the platform (Fig. 8G) compared to untreated or CFA(L) treated APP/PS1 mice. The animal performance could be ranked in order of CA(H) > WT > (CA(L)  $\approx$  AD control).

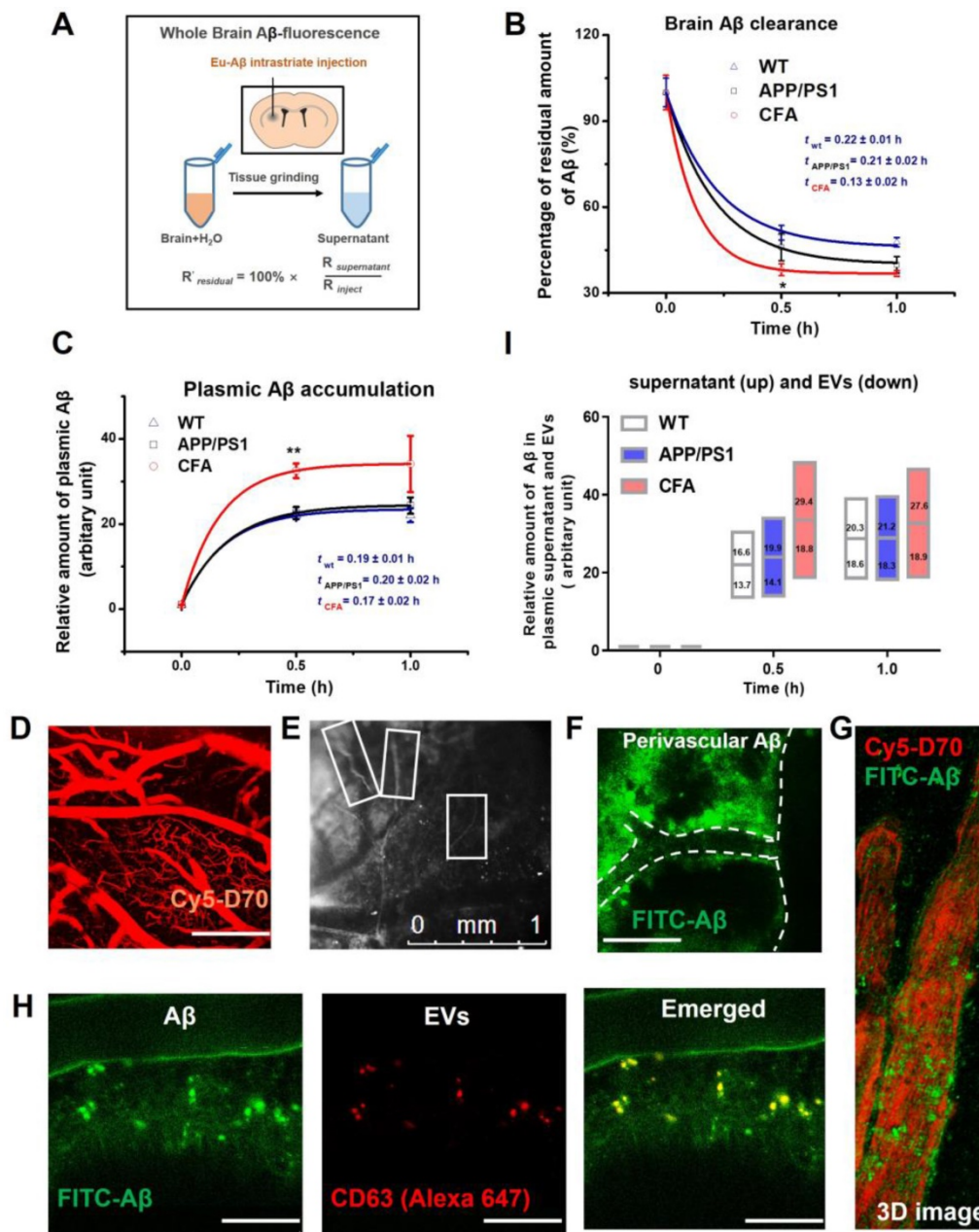


**Figure 7. CFA enhanced brain A $\beta$  excretion in both EVs-bound and unbound forms in APP/PS1 AD mice.** Eu-labeled amyloid  $\beta$  (Eu-A $\beta$ , 2 $\mu$ l) was injected into the mouse striatum and interstitial soluble amyloid A $\beta$  clearing from the brain parenchyma was evaluated as described in Materials and Methods. (A) Schematic of A $\beta$  intrastriatal injection and fluorescence measurement setup. (B) The time course of brain A $\beta$  content (\* $P$  < 0.05,  $n$  = 4–6). (C) Time course of A $\beta$  level in peripheral blood (\*\* $P$  < 0.01,  $n$  = 4–6). The fluorescence intensity of samples was presented as folds of plasma fluorescence blank. (D–H) *In vivo* imaging of A $\beta$  flux in mouse cortex surface layer (0–240  $\mu$ m) after intracisternal injection. D: cerebral vasculature visualized with intra-arterial Cy5-Dextran 70KD. Scale bars, 250  $\mu$ m. < 0.5 h after intracisternal injection. E: capillaries surrounded by FITC-labeled A $\beta$  highlighted by rectangle marks; F: FITC-labeled A $\beta$  (Green) moving along the outside of cerebral surface blood vessels in a representative area (green circle) in F. Scale bars, 250  $\mu$ m. G: 3D image of FITC-A $\beta$  spots (Green) moving outside blood vessels. The fluorescence background of free FITC-A $\beta$  was reduced manually to highlight the A $\beta$  spots. (H) Co-localization of EVs and A $\beta$  spots outside cerebral blood vessels. EVs was visualized with an Alexa 647-labeled CD63 antibody. Scale bars, 50  $\mu$ m. (I) The relative amounts of free plasma A $\beta$  and EVs-bound forms.

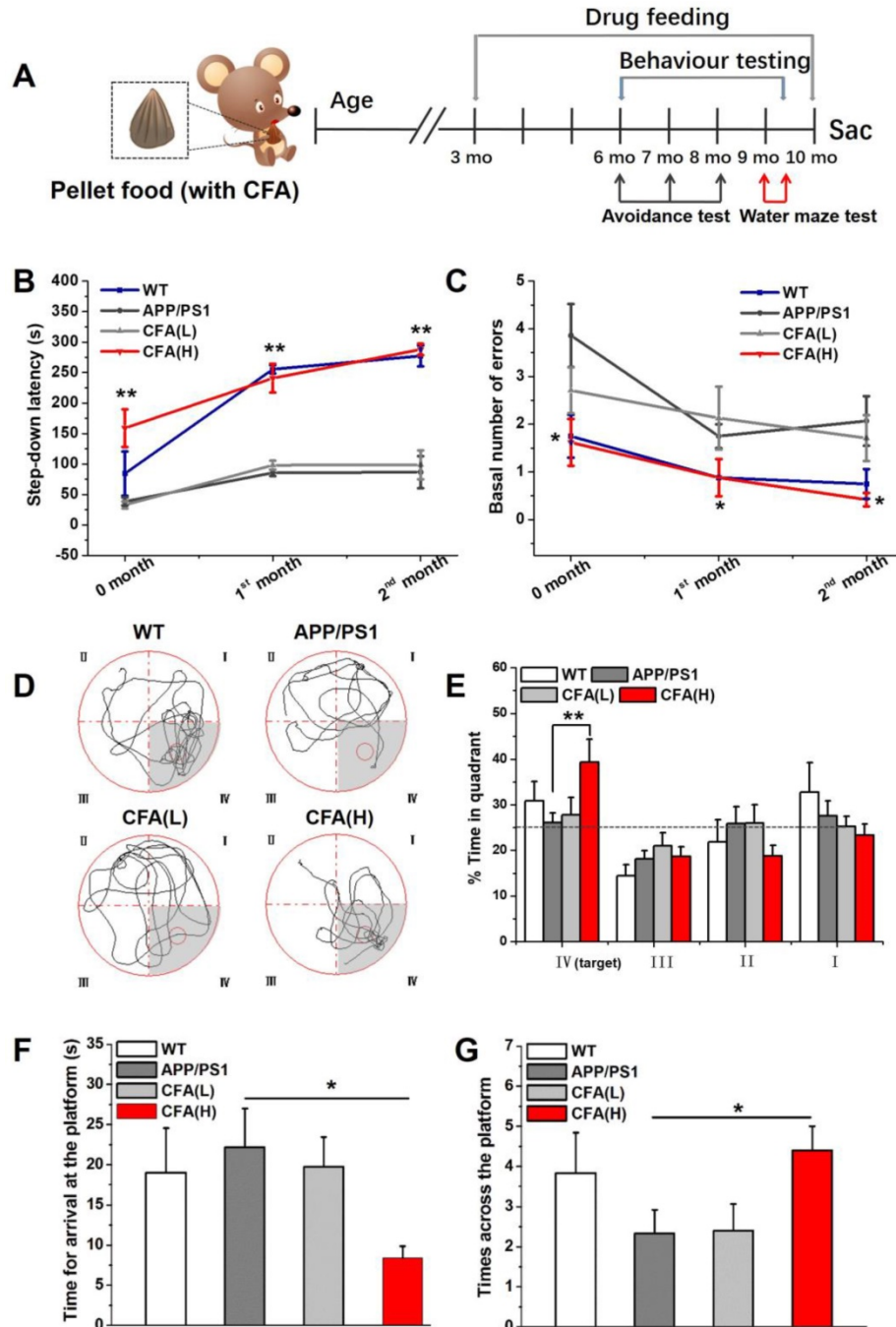
The ability of CFA (0.2 mmol kg<sup>-1</sup>d<sup>-1</sup>) to preserve learning and memory function of female APP/PS1 mice was also assessed (Fig. S9) and similar results were observed as in the male APP/PS1 mice. Overall, the experimental results indicated that APP/PS1 mice had impaired spatial memory compared to WT animals, but high CFA dosage treatment rescued the memory phenotype. Low dosage of CFA was overall ineffective despite improvement in certain aspects.

### Coniferaldehyde prevents neuronal loss in APP/PS1 AD mice.

In untreated male APP/PS1 mice, consistent with previous reports [56, 57], substantial neuronal loss was apparent in the hippocampus (Fig. 9A–C) and in cerebral cortex (Fig. 9D), with many remaining neurons demonstrating basophilic staining and deeply stained and condensed nuclei. In contrast, no

obvious pathological alterations were observed in CFA(H) treated mice (Fig. 9E-H). In addition, the dentate gyrus (DG) of CFA(H)-treated mice showed well preserved holonomic structure similar to WT mice (Fig. S10) and had obviously more cell layers than the untreated APP/PS1 control. When the number of surviving neurons was quantified, both high and low doses of CFA significantly increased the

number of cells observed in the DG compared to WT and untreated APP/PS1 mice (Fig. 9I). In the hippocampus (CA1-CA4), CFA(H) significantly increased the number of surviving neurons (Fig. 9J) and decreased the number of basophilic neurons (Fig. 9K) compared to either WT or untreated APP/PS1 animals.



The results of Nissl staining analysis (Fig. 9L-O) revealed that CFA(H) treatment caused obviously more abundant and larger neuronal Nissl bodies in both hippocampus and cerebral cortex, indicating improvement of structure and functions of neuronal endoplasmic reticulum and golgi apparatus [58, 59] upon treatment with CFA(H).

### Coniferaldehyde prevents toxic A $\beta$ accumulation in APP/PS1 AD mice

A $\beta$  plaques are one important sign in AD pathology [4, 15, 16] recapitulated in the APP/PS1 model. Histological analysis of A $\beta$  peptides revealed significant A $\beta$  plaques in hippocampus, cerebral cortex and cerebellum, and intracellular A $\beta$  staining (Fig. 10A) in untreated APP/PS1, but not WT mice. In comparison, in CFA(H)-treated mice A $\beta$  plaques were

significantly reduced in hippocampus and cerebral cortex, and absent in cerebellum (Fig. 10B).

Because the soluble A $\beta$  oligomers (also known as A $\beta$ -derived diffusible ligands, ADDLs) are suggested as more neurotoxic species [12, 20, 60, 61] than A $\beta$  deposits, the levels of soluble A $\beta$  oligomers upon CFA treatment were determined. The results showed that the amounts of soluble A $\beta$  oligomers in CFA-treated groups were drastically reduced in both hippocampus (Fig. 10C-D) and frontal cortex (Fig. 10E-F) in a dose-dependent manner. Notably, the level of soluble A $\beta$  oligomers in hippocampus of WT mice was elevated despite the lack of A $\beta$  plaques; this may have indicated an aging-related decrease of brain metabolite clearance even in the healthy animals.

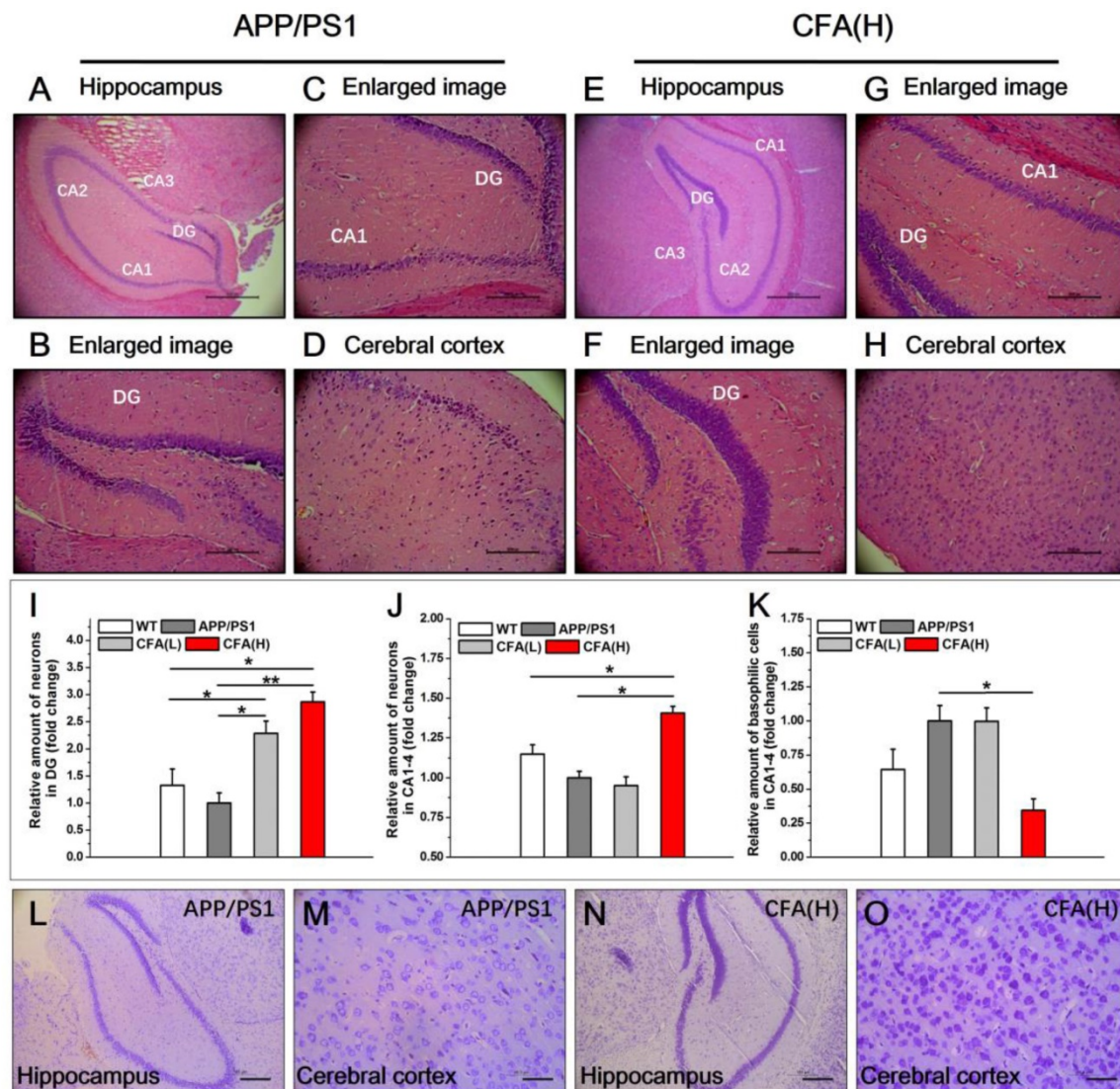


**Figure 9.** Histopathological demonstration of protection effects of CFA in APP/PS1 AD mice. (A-H) Representative images of hematoxylin-eosin (HE) staining of brain sections (hippocampus and cerebral cortex) of APP/PS1 AD model mice (male) upon CFA(H) treatment. Scale bars, 534.5  $\mu$ m for 6.3 $\times$  (A, E), 169.5  $\mu$ m for 20 $\times$  (B-D, F-H). Magnification: 6.3 $\times$  (A, E), 20 $\times$  (B-D, F-H). (I-K) Quantification of the total number of neurons in the DG (I), and the neurons (J) and basophilic cells (K) in CA1, CA2, CA3 and CA4. (L-O) Nissl staining of neurons in the brains APP/PS1 mice upon CFA treatment. Scale bars, 185  $\mu$ m for (L, N); 46.3  $\mu$ m for (M, O). The mice were 10 months old and had been treated with CFA in pellet food for 7 months. Results are mean $\pm$ SE (n=6, with random selection). \*P<0.05, \*\*P<0.01, \*\*\*P<0.001 versus untreated APP/PS1 or specific indication.

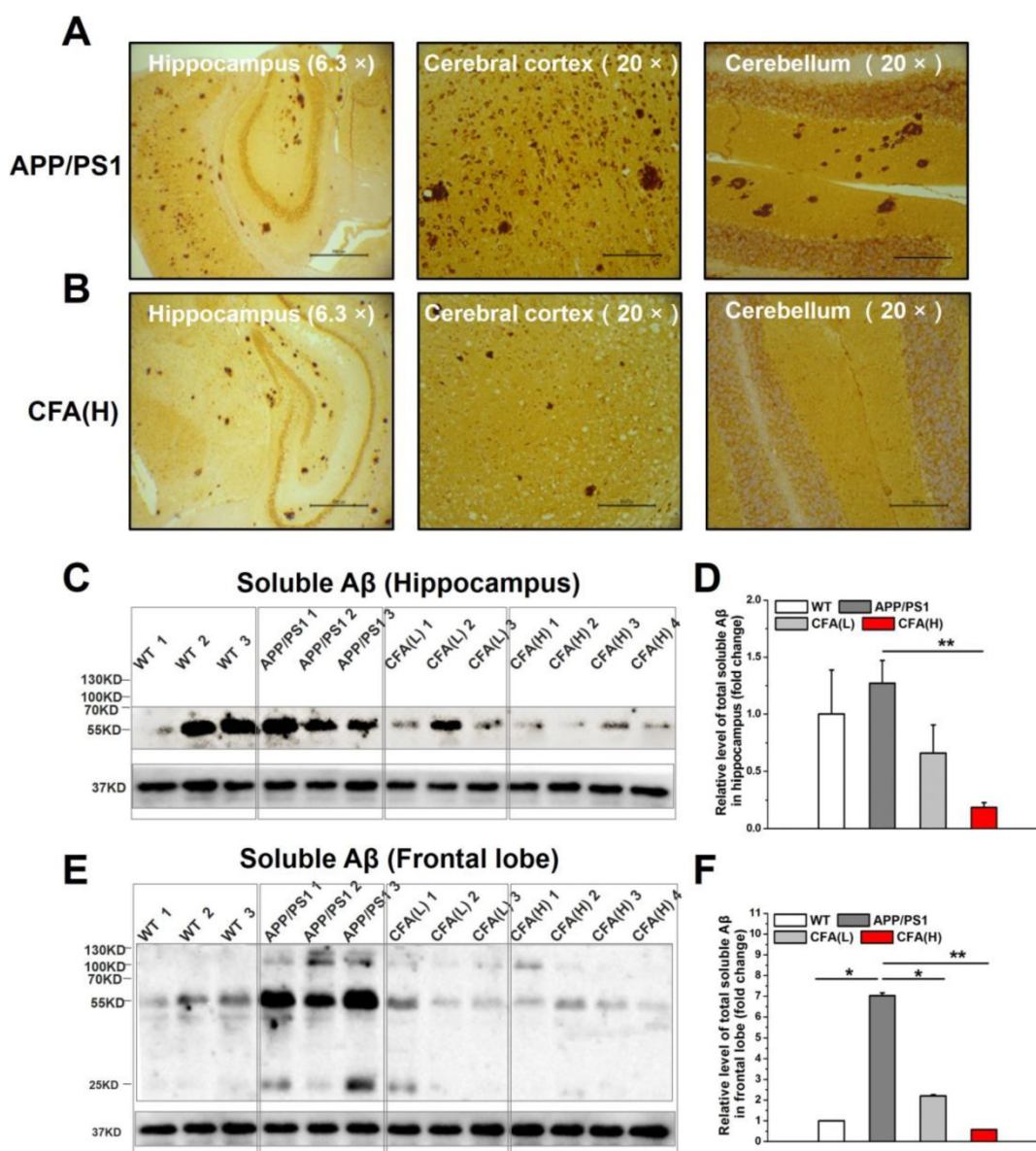


**Figure 10. CFA treatment eliminated brain A $\beta$  deposition and toxic A $\beta$  accumulation.** (A-B) Representative images of brain A $\beta$  deposition. The brain samples (hippocampus, cerebral cortex and cerebellum) were immunostained with the A $\beta$  antibody (6E10) in untreated APP/PS1 control (A) and CFA(H)-treated mice (B). Scale bars, 534.5  $\mu$ m for 6.3 $\times$ , 169.5  $\mu$ m for 20 $\times$ . (C-F) A $\beta$  oligomerization in APP/PS1 mice upon CFA treatment. Western blot analysis and quantification of soluble A $\beta$  peptides in hippocampal lysates (C, D) and frontal lobe lysates (E, F). The mice were 10 months old and had been treated with CFA in pellet food for 7 months. Results are mean $\pm$ SE ( $n=6$ , with random selection). \* $P<0.05$ , \*\* $P<0.01$ , \*\*\* $P<0.001$  versus untreated APP/PS1 or specific indication.

Taken together, the results above demonstrate that CFA treatment effectively promotes brain A $\beta$  clearance and thus attenuates both soluble toxic A $\beta$  levels (Fig. 10C-F) and subsequent insoluble A $\beta$  deposition (Fig. 10B and S11).

## Discussion

The present work aimed to discover safe agents that promote neural cell viability, protect neurons under mitochondrial stress, and can promote A $\beta$  clearance for early stage AD treatment. Considering the role of Nrf2 in regulating major cellular defense systems [21-24], we developed a strategy to screen a series of Nrf2 agonists *in vitro* and revealed promising

properties of CFA. Intriguingly, CFA demonstrated significantly improved the cell viability both with and without A $\beta$  stress or other mitochondrial toxins (MPP<sup>+</sup> and rotenone) (Fig. 1). As expected, CFA strongly activated Nrf2 in neuronal cells both *in vitro* (Fig. 2) and *in vivo* (Fig. 6) and activation of Nrf2 would account for most of the actions of CFA (Fig. 2).

We demonstrate the importance of Nrf2 activation in the neuroprotective effects observed, and hypothesize that its downstream effects are key to the multi-modal, widespread ameliorating effects of CFA on A $\beta$ -induced pathophysiology. Nrf2 is a master transcriptional regulator mediating expression of a variety of antioxidant enzymes and phase II+

enzymes and transporters [21-24, 36, 37]. Under the resting state, Nrf2 is sequestered by Keap1 and targeted for rapid ubiquitin-mediated degradation [21-24, 36, 37]. Upon oxidative stress, Nrf2 is released from Keap1 and phosphorylated, allowing Nrf2 to translocate to the nucleus and start downstream gene expression. Therefore, Nrf2 activation would include signs such as increase of Nrf2 level, nuclear translocation, and expression of downstream genes (e.g. hemeoxygenase 1, HO-1) [21-24, 36-38], all of which were demonstrated in our study upon treatment with CFA. Structurally related molecules, e.g., those containing the  $\alpha,\beta$ -unsaturated carbonyl group, have previously been shown to activate Nrf2 by covalently linking to Keap1, thereby releasing its normal constitutive inhibition of Nrf2 [62, 63], and leading to autoinduction of Nrf2 by its binding to its own promoter. Given the widespread effects of Nrf2 and its downstream targets, it is not surprising that CFA, as an Nrf2 activator, leads to parallel alterations in multiple pathways and cellular functions that are essential in AD pathogenesis [64-66] as demonstrated here. However, the full range of Nrf2 effects, as well as their mechanisms of action mediated by its targets, are an area of active study, and not fully elucidated. Thus, while questions remain about which Nrf2 targets link each of the observed functional improvements, it is quite plausible that this important regulator is a key step in their initiation.

Protection of mitochondrial structure and function is emphasized here because: (i) mitochondria are crucial for cell viability and (ii) are one major target of AD pathogenesis [18, 19, 41]. In fact, bioenergetic deficit is an early aspect of AD pathology closely related to the human disease [18, 19, 41]. Underlying the energy deficiency would be the disruption of the balance of mitochondrial fission and fusion, which leads to mitochondrial fragmentation and reduced mitochondrial density [42-44], and the impairment of mitochondrial oxidative phosphorylation, which causes a shift of the metabolic pattern towards the primitive fermentation of glucose (i.e. glycolysis, as marked by elevation of PKM2) that is similar to the Warburg effect observed in cancer cells [45, 46]. As expected, CFA treatment effectively corrected the morphological and functional alterations in mitochondria induced by A $\beta$  stress (Fig. 3). Further investigation revealed that CFA significantly reduced the level of Drp1 *in vitro* (Fig. 4) and membrane-associated Drp1 *in vivo* (Fig. S5). These results are consistent with previous studies of Drp1 on mitochondrial fragmentation induced by several factors including A $\beta$  stress [48, 49, 67] and suggest that the recovery of mitochondrial morphology likely involves reduced expression or recruitment of Drp1 to

the membrane. CFA treatment also enhanced mitochondrial oxidative phosphorylation capacity (Fig. 3) while reducing A $\beta$ -stimulated glycolysis, including normalization of PKM2 expression (Fig. 4), thus restoring the cellular bioenergetics. However, the detailed mechanisms by which CFA treatment and subsequent Nrf2 activation accomplish these effects remain to be elucidated. A number of pathways by which Nrf2 alters ATP production have been reported, but the effects are dependent on the mechanism of activation, functional context, and cell type [65, 68]. Nonetheless, Nrf2 activation was shown to up-regulate mitochondrial biogenesis genes with effects on improving the efficiency of oxidative phosphorylation and ultimately synthesis of ATP [39, 65], while Nrf2 deficiency would incline mitochondrial energy metabolism toward glycolysis [66]. Hence, while we herein speculated a key role of Nrf2 activation for mitochondrial protection by CFA, its details require further detailed study.

Likely as a result of correcting the structural and functional alteration of mitochondria [69, 70], CFA treatment of SH-SY5Y cells increased the activation of Akt/PKB. Consequently, CFA caused phosphorylation-dependent inactivation of Tau kinase GSK-3 $\beta$  and decrease of p-Tau (S262 and S422) (Fig. 5). These results suggested that CFA is potentially beneficial in reducing tauopathy, though this aspect is waiting for further investigation.

Considering the role of Nrf2 in metabolism and excretion of drugs/wastes/toxins, the effect of CFA on A $\beta$  clearance was tested using an *in vivo* assay (Fig. 7). The results showed that A $\beta$  species were transported from brain to blood in free and EV-bound forms, and CFA treatment significantly improved both the rate and capacity of A $\beta$  excretion (Fig. 7). The detailed pathways for enhanced A $\beta$  excretion by CFA need to be investigated further. Previous works [71, 72] have proposed several mechanisms: blood brain barrier (BBB)-specific efflux, interstitial fluid (ISF) bulk flow and cerebrospinal fluid absorption. Early studies regard BBB as the major pathway for brain A $\beta$  excretion [72]. As Nrf2 up-regulates the endothelial P-glycoprotein (P-gp) [39], CFA might also promote A $\beta$  efflux transport *via* P-gp on BBB. Alternatively, Nedergaard and colleagues recently suggested that ISF bulk flow facilitated by astroglial aquaporin-4 (AQP4) channels (known as the glymphatic system) may contribute to a larger portion of extracellular A $\beta$  clearance [73-77]. As we observed that: (i) about half amount of A $\beta$  species were transported out in EV-bound form and (ii) the A $\beta$  flux moved along the outside space of cortical blood vessels (Fig. 7E-G), the proposed glymphatic drain path [54, 78]. Nonetheless, we expect that clearance of A $\beta$ , whether *via* the BBB or

the glymphatic pathway, to have a major role in the action of CFA.

Together, all the results above prompted us to examine the preventive and protective effects of CFA on AD pathology *in vivo* on the APP/PS1 transgenic mouse, a well-recognized AD animal model [53, 79]. Although APP/PS1 transgenic mice do not recapitulate all aspects of AD pathology, they do undergo amyloid pathogenesis. Observable amyloid deposition begins at the age of 4~5 months and behavioral deficits after 6 months [80, 81]. Importantly, certain crucial neuronal functions, i.e., inactive Nrf2, are quite similar to that of AD patients (Fig. 6). In addition, other important aspects of AD pathology such as Tau hyperphosphorylation normally appear in the later stages following A $\beta$  overproduction [50, 51]. Thus, the APP/PS1 transgenic mouse model is quite suitable for observing the effects of AD preventive drugs on the elevation of amyloid and its consequences, whether as initiating events or key elements facilitating AD progress in the early stages of AD [4, 18, 19, 41].

We started dosing animals with CFA at 3 months (Fig. 8A) when amyloid deposits are not observable, but the mice already exhibit early pathological changes, i.e. swollen cholinergic axons and cholinesterase positive reactions in the cortex and hippocampus [79, 82-84]. The results were of note: (i) CFA at the effective dosage (0.2 mmol kg<sup>-1</sup>day<sup>-1</sup>) effectively preserved learning and memory function of the model mice (Fig. 8). (ii) CFA treatment significantly reduced AD-like pathological amyloid features (Fig. 9 and 10), i.e. well-preserved DG holonomic structure, improved number of surviving neurons, decreased the number of basophilic cells and improved neuronal endoplasmic reticulum and golgi apparatus, etc.; (iii) CFA treatment almost cleaned the A $\beta$  deposits in major brain regions (Fig. 10 and S11) and essentially abolished the toxic soluble A $\beta$  species (Fig. 10), which conceivably could account for the reduction of neuronal lesions and improved cognitive function.

Another noteworthy effect of CFA is the recovery of Nrf2 activity *in vivo* (Fig. 6). Previously, Nrf2 was found inactive in AD brain despite the presence of oxidative stress [25, 26]. Conceivably, several Nrf2-dependent antioxidant enzymes such as SOD1 and catalase were also found reduced in human AD brains [26, 85]. In APP/PS1 mice, overexpression of Nrf2 protected neurons against A $\beta$  toxicity and recovered spatial learning [22, 26, 66] but knockout of Nrf2 aggravated oxidative damage [86]. Herein, we found that Nrf2 was down-regulated A $\beta$ -expressing neural cells (Fig. S3), while in APP/PS1 mice, Nrf2 was both down-regulated and inactive (Fig. 6).

Moreover, brain A $\beta$  excretion in APP/PS1 mice showed a reduced rate (Fig. 7). Hence, we expect a major role of Nrf2 activation in the action of CFA despite lack of elucidation of the detailed pathways in the future works. Nevertheless, the present work supports Nrf2 as an enticing target for AD therapeutic agent discovery.

The preventive/protective effects of CFA *in vitro* and animal models suggest further studies of CFA in human subjects, especially in patients already diagnosed with cognitive impairment. An important benefit of CFA as a potential AD treatment is that it is a legal food flavoring (EFSA FL-No. 05.155), essential in wine brandy/whiskey [29, 87]. CFA is also an active ingredient in many herbals, such as propolis and bamboo shavings. Analysis of brain CFA concentrations in mice upon oral administration (0.2 mmol/kg) revealed a quick absorption of CFA with a peak at about 1h (Fig. S12) and the data may fit into a compartmental pharmacokinetic model, suggesting that CFA can easily pass through BBB. More importantly, CFA shows a safety profile (Oral LD50: mouse, 300 mg/kg; rabbit 3200 mg/kg; rat, 980 mg/kg) well within the effective range tested here. This factor is especially appealing for a potential preventative medication, as administration to patients not currently exhibiting severe disease particularly requires high safety and low side effects.

In summary, the current investigation demonstrates that a food flavoring CFA, when given during early stages of AD-related processes, could greatly diminish amyloid pathogenesis in APP/PS1 transgenic mice. The mechanism of the actions of CFA involved protective actions probably include the protection of mitochondrial structure, dynamics, and energy metabolism from A $\beta$  toxicity particularly as well as enhancement of A $\beta$  excretion. The enhanced A $\beta$  secretion is likely *via* the glymphatic and/or BBB efflux systems in both free and exosomes and microvesicles (EVs)-bound forms, emphasizing the need of further investigation on EVs in A $\beta$  transportation. Furthermore, our results overall support Nrf2 activation as an essential mechanism for the therapeutic effects of CFA. With good safety and pharmacokinetic profiles, CFA would be an ideal candidate for further clinical tests as a preventative medicine of AD.

## Abbreviations

ADDLs: A $\beta$ -derived diffusible ligands; APP: amyloid precursor protein; APP/PS1: APP<sup>swE</sup>/PS1<sup>dE9</sup>; ATRA: all-trans-retinoic acid; CFA: coniferaldehyde; DG: dentate gyrus; MPP<sup>+</sup>: 1-methyl-4-phenylpyridinium; Nrf2: NF-E2-related

factor 2; MWM: Morris water maze; Rot: Rotenone; WT: wild type.

## Supplementary Material

Supplementary methods and figures.  
<http://www.thno.org/v10p0179s1.pdf>

## Acknowledgements

This work was supported by the National Natural Science Foundation of China (#21571006, #21771010 and #81671187), National Key Technology Research and Development Program of China (No. 2016YFC1306500), Beijing Municipal Science & Technology Commission (Z171100000117013, Z161100000216150), the “Strategic Priority Research Program” of the Chinese Academy of Sciences (XDA 12040101) and National Institutes of Health (R01 AG056711). We thank Dr. Zengqiang Yuan at the Institute of Biophysic, Chinese Academy of Sciences for providing the three SH-SY5Y cells and kindly assistances in cell culture.

## Author Contributions

JZ and XD-Y were responsible for the conception and design of the study. YQ-D conducted the study, analyzed the data and wrote the original draft of the manuscript. JZ, XD-Y, YQ-D, TS, JI and MS provided critical review of the manuscript. YQ-D was involved in all of the experiments. LD-B and XL were involved in the MTS studies. TX and LY were involved in lymphatic drainage system studies. DF-Z was involved in the brain histology and immunohistochemistry studies. TT-W was involved in mitochondrial OCR and EACR studies. All authors read and approved the final manuscript.

## Competing Interests

The authors have declared that no competing interest exists.

## References

- Galvin JE, Howard DH, Denny SS, Dickinson S, Tatton N. The social and economic burden of frontotemporal degeneration. *Neurology*. 2017; 89: 2049-56
- Morrison C. Hope for anti-amyloid antibodies surges, yet again. *Nat Biotechnol*. 2016; 34: 1082-3.
- Gold M. Phase II clinical trials of anti-amyloid beta antibodies: When is enough, enough? *Alzheimers Dement (N Y)*. 2017; 3: 402-9.
- Koss DJ, Jones G, Cranston A, Gardner H, Kanaan NM, Platt B. Soluble pre-fibrillar tau and beta-amyloid species emerge in early human Alzheimer's disease and track disease progression and cognitive decline. *Acta Neuropathol*. 2016; 132: 875-95.
- Luo J, Warmlander SK, Graslund A, Abrahams JP. Cross-interactions between the Alzheimer Disease Amyloid-beta Peptide and Other Amyloid Proteins: A Further Aspect of the Amyloid Cascade Hypothesis. *J Biol Chem*. 2016; 291: 16485-93.
- Knight WD, Okello AA, Ryan NS, Turkheimer FE, Rodriguez Martinez de Llano S, Edison P, et al. Carbon-11-Pittsburgh compound B positron emission tomography imaging of amyloid deposition in presenilin 1 mutation carriers. *Brain*. 2011; 134: 293-300.

- Sorrells SF, Paredes MF, Cebrian-Silla A, Sandoval K, Qi D, Kelley KW, et al. Human hippocampal neurogenesis drops sharply in children to undetectable levels in adults. *Nature*. 2018; 555: 377-81.
- Gandy S. PERSPECTIVE Prevention is better than cure. *Nature*. 2011; 475: S15-S15.
- Karran E, Mercken M, Strooper BD. The amyloid cascade hypothesis for Alzheimer's disease: an appraisal for the development of therapeutics. *Nat Rev Drug Discov*. 2011;10: 698-712.
- Lustbader JW, Cirilli M, Lin C, Xu HW, Takuma K, Wang N, et al. ABAD directly links A beta to mitochondrial toxicity in Alzheimer's disease. *Science*. 2004; 304: 448-52.
- Tonnie E, Trushina E. Oxidative Stress, Synaptic Dysfunction, and Alzheimer's Disease. *J Alzheimers Dis*. 2017; 57: 1105-21.
- Umeda T, Ono K, Sakai A, Yamashita M, Mizuguchi M, Klein WL, et al. Rifampicin is a candidate preventive medicine against amyloid-beta and tau oligomers. *Brain*. 2016; 139: 1568-86.
- Du H, Guo L, Fang F, Chen D, Sosunov AA, McKhann GM, et al. Cyclophilin D deficiency attenuates mitochondrial and neuronal perturbation and ameliorates learning and memory in Alzheimer's disease. *Nat Med*. 2008; 14: 1097-105.
- Hirai K, Aliev G, Nunomura A, Fujioka H, Russell RL, Atwood CS, et al. Mitochondrial abnormalities in Alzheimer's disease. *J Neurosci*. 2001; 21: 3017-23.
- Glabbe CG. Structural classification of toxic amyloid oligomers. *J Biol Chem*. 2008; 283: 29639-43.
- Glabbe CG. Common mechanisms of amyloid oligomer pathogenesis in degenerative disease. *Neurobiol Aging*. 2006; 27: 570-5.
- Mawuenyega KG, Sigurdson W, Ovod V, Munsell L, Kasten T, Morris JC, et al. Decreased clearance of CNS beta-amyloid in Alzheimer's disease. *Science*. 2010; 330: 1774.
- Lin MT, Beal MF. Mitochondrial dysfunction and oxidative stress in neurodegenerative diseases. *Nature*. 2006; 443: 787-95.
- Beck SJ, Guo L, Phensy A, Tian J, Wang L, Tandon N, et al. Deregulation of mitochondrial FIFO-ATP synthase via OSCP in Alzheimer's disease. *Nat Commun*. 2016; 7: 11483.
- Voorhees JR, Remy MT, Cintron-Perez CJ, El Rassi E, Khan MZ, Dutca LM, et al. (-)-P7C3-S243 Protects a Rat Model of Alzheimer's Disease From Neuropsychiatric Deficits and Neurodegeneration Without Altering Amyloid Deposition or Reactive Glia. *Biol Psychiatry*. 2018; 84: 488-98.
- Johnson DA, Johnson JA. Nrf2—a therapeutic target for the treatment of neurodegenerative diseases. *Free Radic Biol Med*. 2015; 88: 253-67.
- Jhang KA, Lee EO, Kim HS, Chong YH. Norepinephrine provides short-term neuroprotection against Abeta1-42 by reducing oxidative stress independent of Nrf2 activation. *Neurobiol Aging*. 2014; 35: 2465-73.
- Johnson JA, Johnson DA, Kraft AD, Calkins MJ, Jakel RJ, Vargas MR, et al. The Nrf2-ARE pathway: an indicator and modulator of oxidative stress in neurodegeneration. *Ann N Y Acad Sci*. 2008; 1147: 61-9.
- Dinkova-Kostova AT, Abramov AY. The emerging role of Nrf2 in mitochondrial function. *Free Radic Biol Med*. 2015; 88: 179-88.
- Ramsey CP, Glass CA, Montgomery MB, Lindl KA, Ritson GP, Chia LA, et al. Expression of Nrf2 in neurodegenerative diseases. *J Neuropath Exp Neur*. 2007; 66: 75-85.
- Murphy KE, Park JJ. Can Co-Activation of Nrf2 and Neurotrophic Signaling Pathway Slow Alzheimer's Disease? *Int J Mol Sci*. 2017; 18: 1168-95.
- Peterson DW, George RC, Scaramozzino F, LaPointe NE, Anderson RA, Graves DJ, et al. Cinnamon extract inhibits tau aggregation associated with Alzheimer's disease in vitro. *J Alzheimers Dis*. 2009; 17: 585-97.
- George RC, Lew J, Graves DJ. Interaction of cinnamaldehyde and epicatechin with tau: implications of beneficial effects in modulating Alzheimer's disease pathogenesis. *J Alzheimers Dis*. 2013; 36: 21-40.
- Panossian A, Mamikonyan G, Torosyan M, Gabrielyan E, Mkhitaryan S. Analysis of aromatic aldehydes in brandy and wine by high-performance capillary electrophoresis. *Anal Chem*. 2001; 73: 4379-83.
- Itoh T, Ando M, Tsukamasa Y, Wakimoto T, Nukaya H. Whiskey Congeners Suppress LPS/IFN gamma-Induced NO Production in Murine Macrophage RAW 264 Cells by Inducing Heme Oxygenase-1 Expression. *J Agr Food Chem*. 2012; 60: 12491-500.
- Zhang J, Liu Q, Chen Q, Liu NQ, Li FL, Lu ZB, et al. Nicotine attenuates beta-amyloid-induced neurotoxicity by regulating metal homeostasis. *FASEB J*. 2006; 20: 1212-4.
- Malich G, Markovic B, Winder C. The sensitivity and specificity of the MTS tetrazolium assay for detecting the in vitro cytotoxicity of 20 chemicals using human cell lines. *Toxicology*. 1997; 124: 179-92.
- Zhang B, Chu W, Wei P, Liu Y, Wei T. Xanthohumol induces generation of reactive oxygen species and triggers apoptosis through inhibition of

- mitochondrial electron transfer chain complex I. *Free Radic Biol Med.* 2015; 89: 486-97.
34. Xu ZH, Zhang CY, Zhang Y, Yang XD. Europium Complexes as Novel Indicators of Paracellular Diffusion. *Chem Biodivers.* 2012; 9: 1916-22.
  35. Port RE, Knopp MV, Brix G. Dynamic contrast-enhanced MRI using Gd-DTPA: interindividual variability of the arterial input function and consequences for the assessment of kinetics in tumors. *Magn Reson Med.* 2001; 45: 1030-8.
  36. Kerr F, Sofola-Adesakin O, Ivanov DK, Gatliff J, Gomez Perez-Nievas B, Bertrand HC, et al. Direct Keap1-Nrf2 disruption as a potential therapeutic target for Alzheimer's disease. *PLoS Genet.* 2017; 13: e1006593.
  37. Merchant AA, Singh A, Matsui W, Biswal S. The redox-sensitive transcription factor Nrf2 regulates murine hematopoietic stem cell survival independently of ROS levels. *Blood.* 2011; 118: 6572-9.
  38. Biswas C, Shah N, Muthu M, La P, Fernando AP, Sengupta S, et al. Nuclear heme oxygenase-1 (HO-1) modulates subcellular distribution and activation of Nrf2, impacting metabolic and anti-oxidant defenses. *J Biol Chem.* 2014; 289: 26882-94.
  39. Wang X, Campos CR, Peart JC, Smith LK, Boni JL, Cannon RE, et al. Nrf2 upregulates ATP binding cassette transporter expression and activity at the blood-brain and blood-spinal cord barriers. *J Neurosci.* 2014; 34: 8585-93.
  40. Wang XJ, Hayes JD, Henderson CJ, Wolf CR. Identification of retinoic acid as an inhibitor of transcription factor Nrf2 through activation of retinoic acid receptor alpha. *Proc Natl Acad Sci U S A.* 2007; 104: 19589-94.
  41. Cardoso SM, Santana I, Swerdlow RH, Oliveira CR. Mitochondria dysfunction of Alzheimer's disease cybrids enhances A beta toxicity. *J Neurochem.* 2004; 89: 1417-26.
  42. Zhu X, Perry G, Smith MA, Wang X. Abnormal mitochondrial dynamics in the pathogenesis of Alzheimer's disease. *J Alzheimers Dis.* 2013; 33 Suppl 1: S253-62.
  43. Chen Q, Zhang J, Zhao K, Li W, Miao Q, Sun Y, et al. Lysosomal chymotrypsin induces mitochondrial fission in apoptotic cells by proteolytic activation of calcineurin. *Protein Cell.* 2014; 5: 643-7.
  44. Gray NE, Sampath H, Zweig JA, Quinn JF, Soumyanath A. Centella asiatica Attenuates Amyloid-beta-Induced Oxidative Stress and Mitochondrial Dysfunction. *J Alzheimers Dis.* 2015; 45: 933-46.
  45. Chaneton B, Gottlieb E. Rocking cell metabolism: revised functions of the key glycolytic regulator PKM2 in cancer. *Trends Biochem Sci.* 2012; 37: 309-16.
  46. Martire S, Fusco A, Mosca L, Forte E, Correani V, Fontana M, et al. Bioenergetic Impairment in Animal and Cellular Models of Alzheimer's Disease: PARP-1 Inhibition Rescues Metabolic Dysfunctions. *J Alzheimers Dis.* 2016; 54: 307-24.
  47. Wallace DC. Mitochondrial diseases in man and mouse. *Science.* 1999; 283: 1482-8.
  48. Grohm J, Kim SW, Mamrak U, Tobaben S, Cassidy-Stone A, Nunnari J, et al. Inhibition of Drp1 provides neuroprotection in vitro and in vivo. *Cell Death Differ.* 2012; 19: 1446-58.
  49. Wang X, Su B, Siedlak SL, Moreira PI, Fujioka H, Wang Y, et al. Amyloid-beta overproduction causes abnormal mitochondrial dynamics via differential modulation of mitochondrial fission/fusion proteins. *Proc Natl Acad Sci U S A.* 2008; 105: 19318-23.
  50. Arriagada PV, Growdon JH, Hedley-Whyte ET, Hyman BT. Neurofibrillary tangles but not senile plaques parallel duration and severity of Alzheimer's disease. *Neurology.* 1992; 42: 631-9.
  51. Goedert M. NEURODEGENERATION. Alzheimer's and Parkinson's diseases: The prion concept in relation to assembled Abeta, tau, and alpha-synuclein. *Science.* 2015; 349: 1255555.
  52. Takashima A. GSK-3 is essential in the pathogenesis of Alzheimer's disease. *J Alzheimers Dis.* 2006; 9: 309-17.
  53. Borchelt DR, Thinakaran G, Eckman CB, Lee MK, Davenport F, Ratovitsky T, et al. Familial Alzheimer's disease-linked presenilin 1 variants elevate Abeta1-42/1-40 ratio in vitro and in vivo. *Neuron.* 1996; 17: 1005-13.
  54. Iliff JJ, Wang MH, Liao YH, Plogg BA, Peng WG, Gundersen GA, et al. A Paravascular Pathway Facilitates CSF Flow Through the Brain Parenchyma and the Clearance of Interstitial Solutes, Including Amyloid beta. *Sci Transl Med.* 2012; 4: 147ra111.
  55. Rajendran L, Honsho M, Zahn TR, Keller P, Geiger KD, Verkade P, et al. Alzheimer's disease beta-amyloid peptides are released in association with exosomes. *Proc Natl Acad Sci U S A.* 2006; 103: 11172-7.
  56. Schoene-Bake JC, Keller SS, Niehusmann P, Volmering E, Elger C, Deppe M, et al. In vivo mapping of hippocampal subfields in mesial temporal lobe epilepsy: relation to histopathology. *Hum Brain Mapp.* 2014; 35: 4718-28.
  57. Roy DS, Arons A, Mitchell TI, Pignatelli M, Ryan TJ, Tonegawa S. Memory retrieval by activating engram cells in mouse models of early Alzheimer's disease. *Nature.* 2016; 531: 508-12.
  58. Richard FT. *The brain: A neuroscience primer*, (2nd edn). New York, USA: W. H. Freeman; 1993.
  59. Braun N, Schikorski T, Zimmermann H. Cytoplasmic segregation and cytoskeletal organization in the electric catfish giant electromotoneuron with special reference to the axon hillock region. *Neuroscience.* 1993; 52: 745-56.
  60. Camilleri A, Zarb C, Caruana M, Ostermeier U, Ghio S, Hogen T, et al. Mitochondrial membrane permeabilisation by amyloid aggregates and protection by polyphenols. *Biochimica Et Biophysica Acta.* 2013; 1828: 2532-43.
  61. Kaye R, Sokolov Y, Edmonds B, McIntire TM, Milton SC, Hall JE, et al. Permeabilization of lipid bilayers is a common conformation-dependent activity of soluble amyloid oligomers in protein misfolding diseases. *J Biol Chem.* 2004; 279: 46363-6.
  62. Wu RP, Hayashi T, Cottam HB, Jin G, Yao S, Wu CC, et al. Nrf2 responses and the therapeutic selectivity of electrophilic compounds in chronic lymphocytic leukemia. *Proc Natl Acad Sci U S A.* 2010; 107: 7479-84.
  63. Magesh S, Chen Y, Hu L. Small molecule modulators of Keap1-Nrf2-ARE pathway as potential preventive and therapeutic agents. *Med Res Rev.* 2012; 32: 687-726.
  64. Wang XQ, Campos CR, Peart JC, Smith LK, Boni JL, Cannon RE, et al. Nrf2 Upregulates ATP Binding Cassette Transporter Expression and Activity at the Blood-Brain and Blood-Spinal Cord Barriers. *J Neurosci.* 2014; 34: 8585-93.
  65. Holmstrom KM, Baird L, Zhang Y, Hargreaves I, Chalasani A, Land JM, et al. Nrf2 impacts cellular bioenergetics by controlling substrate availability for mitochondrial respiration. *Biol Open.* 2013; 2: 761-70.
  66. Jan A, Jansonius B, Delaidelli A, Somasekharan SP, Bhanshali F, Vandal M, et al. eEF2K inhibition blocks Abeta42 neurotoxicity by promoting an NRF2 antioxidant response. *Acta Neuropathol.* 2017; 133: 101-19.
  67. Mears JA, Lackner LL, Fang S, Ingeman E, Nunnari J, Hinshaw JE. Conformational changes in Dnm1 support a contractile mechanism for mitochondrial fission. *Nat Struct Mol Biol.* 2011; 18: 20-6.
  68. Sajja RK, Kaisar MA, Vijay V, Desai VG, Prasad S, Cuccullo L. In Vitro Modulation of Redox and Metabolism Interplay at the Brain Vascular Endothelium: Genomic and Proteomic Profiles of Sulforaphane Activity. *Sci Rep.* 2018; 8: 12708.
  69. Kim JH, Go HY, Jin DH, Kim HP, Hong MH, Chung WY, et al. Inhibition of the PI3K-Akt/PKB survival pathway enhanced an ethanol extract of *Rhus verniciflua* Stokes-induced apoptosis via a mitochondrial pathway in AGS gastric cancer cell lines. *Cancer Lett.* 2008; 265: 197-205.
  70. Vander Haar E, Lee SI, Bandhakavi S, Griffin TJ, Kim DH. Insulin signalling to mTOR mediated by the Akt/PKB substrate PRAS40. *Nat Cell Biol.* 2007; 9: 316-23.
  71. Tarasoff-Conway JM, Carare RO, Osorio RS, Glodzik L, Butler T, Fieremans E, et al. Clearance systems in the brain-implications for Alzheimer disease. *Nat Rev Neurol.* 2015; 11: 457-70.
  72. Shibata M, Yamada S, Kumar SR, Calero M, Bading J, Frangione B, et al. Clearance of Alzheimer's amyloid-beta(1-40) peptide from brain by LDL receptor-related protein-1 at the blood-brain barrier. *J Clin Invest.* 2000; 106: 1489-99.
  73. Nedergaard M. Garbage Truck of the Brain. *Science.* 2013; 340: 1529-30.
  74. Iliff JJ, Nedergaard M. Is There a Cerebral Lymphatic System? *Stroke.* 2013; 44: S93-55.
  75. Jessen NA, Munk ASF, Lundgaard I, Nedergaard M. The Glymphatic System: A Beginner's Guide. *Neurochem Res.* 2015; 40: 2583-99.
  76. Sun BL, Wang LH, Yang T, Sun JY, Mao LL, Yang MF, et al. Lymphatic drainage system of the brain: A novel target for intervention of neurological diseases. *Prog Neurobiol.* 2018; 163-164: 118-43.
  77. Mestre H, Hablitz LM, Xavier AL, Feng W, Zou W, Pu T, et al. Aquaporin-4-dependent glymphatic solute transport in the rodent brain. *eLife.* 2018; 7: e40070.
  78. Madigan JB, Wilcock DM, Hainsworth AH. Vascular Contributions to Cognitive Impairment and Dementia: Topical Review of Animal Models. *Stroke.* 2016; 47: 1953-9.
  79. Duyckaerts C, Potier MC, Delatour B. Alzheimer disease models and human neuropathology: similarities and differences. *Acta Neuropathol.* 2008; 115: 5-38.
  80. Jankowsky JL, Slunt HH, Ratovitsky T, Jenkins NA, Copeland NG, Borchelt DR. Co-expression of multiple transgenes in mouse CNS: a comparison of strategies. *Biomol Eng.* 2001; 17: 157-65.
  81. Garcia-Alloza M, Robbins EM, Zhang-Nunes SX, Purcell SM, Betensky RA, Raju S, et al. Characterization of amyloid deposition in the APP<sup>swE</sup>/PS1<sup>dE9</sup> mouse model of Alzheimer disease. *Neurobiol Dis.* 2006; 24: 516-24.

82. Lee JE, Han PL. An update of animal models of Alzheimer disease with a reevaluation of plaque depositions. *Exp Neurobiol.* 2013; 22: 84-95.
83. Wilcock DM, Colton CA. Anti-amyloid-beta immunotherapy in Alzheimer's disease: relevance of transgenic mouse studies to clinical trials. *J Alzheimers Dis.* 2008; 15: 555-69.
84. Ruan L, Kang Z, Pei G, Le Y. Amyloid deposition and inflammation in APP<sup>swE</sup>/PS1<sup>dE9</sup> mouse model of Alzheimer's disease. *Curr Alzheimer Res.* 2009; 6: 531-40.
85. Rojo AI, Pajares M, Rada P, Nunez A, Nevado-Holgado AJ, Killik R, et al. NRF2 deficiency replicates transcriptomic changes in Alzheimer's patients and worsens APP and TAU pathology. *Redox Biol.* 2017; 13: 444-51.
86. Joshi G, Gan KA, Johnson DA, Johnson JA. Increased Alzheimer's disease-like pathology in the APP/ PS1<sup>DeltaE9</sup> mouse model lacking Nrf2 through modulation of autophagy. *Neurobiol Aging.* 2015; 36: 664-79.
87. Choi SK, Mun GI, Choi E, Kim SY, Kwon Y, Na Y, et al. The Conjugated Double Bond of Coniferyl Aldehyde Is Essential for Heat Shock Factor 1 Mediated Cytotoprotection. *J Nat Prod.* 2017; 80: 2379-83.